Geophys. J. Int. (2006) **165,** 1041–1057 doi: 10.1111/j.1365-246X.2006.02990.x

Influence of past and present-day plate motions on spherical models of mantle convection: implications for mantle plumes and hotspots

Sandrine Quéré and Alessandro M. Forte

GEOTOP, Département des Sciences de la Terre, Cp. 8888, *succ. centre ville, Montréal, Québec,* H3C-3P8, *Canada. E-mail: squere@sca.uqam.ca*

Accepted 2006 March 6. Received 2006 March 4; in original form 2005 April 18

SUMMARY

We explore the influence of tectonic plate motions, given by the no-net-rotation (NNR)-NUVEL-1 model, on a 3-D spherical model of mantle convection in which plates can be coupled to the underlying mantle flow in a dynamically consistent manner. We first derived a reference convection model in which only the NUVEL-1 geometry of the tectonic plates is prescribed. The plate rotations are then predicted on the basis of the buoyancy forces in the mantle, ensuring a dynamical balance of torques acting on the plates. This dynamically consistent reference convection model, which is based on a simple two-layer viscosity profile, yields the main features of plate tectonics: linear subduction zones, passive diverging zones and four mantle plumes. We next developed a time-dependent convection model, which is initiated with the average radial temperature field extracted from the reference convection model, and in which we imposed the NNR-NUVEL-1 plate velocities. This convection simulation yields six focused upwelling plumes, whose location and number is very similar to the primary terrestrial hotspots which have been recently identified (Courtillot *et al.* 2003). In all convection models incorporating the NNR-NUVEL-1 plate motions, we find that the surface heat flow and mantle potential temperature stay essentially constant, demonstrating the compatibility between the observed NNR-NUVEL-1 velocities and the internal buoyancy forces in the mantle. To determine the robustness of these results we carried out complementary convection simulations incorporating the past 120 Ma history of tectonic plate evolution. These simulations yielded shifting 'hotlines' at the core–mantle boundary, but the locations of the overlying hotspot plumes remained relatively stable. The configuration of the hotlines in the convection experiments with and without evolving surface plate geometries are very similar to each other, showing that convection models with present-day plate configurations are sufficient for capturing the essential characteristics of the present-day thermal structure in the mantle. In a final experiment, the prescribed NNR-NUVEL-1 plate velocity constraint is released, allowing the plates to rotate freely in response to the underlying mantle flow. We find that the initial evolution of this model is characterized by a strong stability of the mantle thermal structures, in particular the upwelling plumes. An important and novel feature of the convection model with free plate motions is the predicted opening of the African plate along the East African Rift boundary, which occurs in response to the large-scale mantle flow and does not appear to require the presence of upwelling plumes directly beneath the rift.

Key words: African rift, Cenozoic plate motions, hotspots, mantle plumes, NUVEL-1, tectonic plates, thermal convection.

1 INTRODUCTION

The number, identification, interpretation and even the definition of hotspots has been a subject of past and ongoing debate and controversy (Anderson & Natland 2005). (An extensive collection of studies, which address the hotspot debate may be found in www.mantleplumes.org). The concept of 'hotspot' was introduced by Wilson (1963) and the idea was later extended by Morgan (1971, 1972), who proposed the fixity of hotspots, and hence a new reference frame for plate motions, on the assumption that hotspots are the surface expressions of focused hot upwellings originating in the lower mantle.

The early inventories of terrestrial hotspots included as many as 20 (Morgan 1972), but their identification is subject to considerable interpretation, depending on various combinations of geological and geophysical criteria (Anderson 2005). The number of

identified hotspots has, therefore, varied over the years, the tendency being towards an increase in their number. For example, on the basis of buoyancy flux estimates, as many as 40 hotspots have been identified as significant (Sleep 1990), but according to the multiple ranking criteria employed by Courtillot *et al.* (2003), there are only seven primary hotspots from a total number of 49. About 20 of the less significant hotspots are attributed to plumes originating on top of transient domes at intermediate mantle depths (Davaille 1999), while another 20 might be linked to shallow asthenospheric convection (Anderson 2000).

Seismic tomographic imaging of the depth, morphology and mantle source regions of the terrestrial hotspots is difficult and often ambiguous (Keller *et al.* 2000) but considerable progress has been made over the past few years (Nataf 2000; Garnero 2000). On Earth, the Hawaii, Iceland and perhaps the Réunion hotspots are classified as 'isolated', in contrast to the other terrestrial hotspots (e.g. in the Pacific superswell) which occur in groups or clusters (Sleep 1990). Previous seismic studies of the isolated Hawaii hotspot have suggested a lower-mantle origin for the corresponding thermal plume (Li *et al.* 2000), which may extend down to the core–mantle boundary (CMB) (Russell *et al.* 1998). Similar seismic studies of the isolated Iceland hotspot have suggested a variety of source depths for the associated mantle plume, ranging from the upper-mantle (Wolfe *et al.* 1997; Foulger *et al.* 2001) to the lower-mantle (Shen *et al.* 1998), and possibly extending to the CMB (Helmberger *et al.* 1998). A recent global seismic tomographic study of the structure of the plume conduits below hotspots has again highlighted the difficulty in obtaining sufficient deep-mantle resolution (e.g. below Hawaii) with the current global seismic data (Montelli *et al.* 2004).

The theoretical, numerical and experimental modelling of mantle plumes in thermal convective flows has a long and rich history which cannot be adequately covered in the present discussion. References to some of the classical studies may be found in Whitehead (1988) and also in www.mantleplumes.org. The most relevant recent studies, which have a direct bearing on the plume modelling presented below are the numerical convection simulations (in alphabetical order) by: Bunge *et al.* (1998, 2002), Labrosse (2002), Lowman *et al.* (2001), Monnereau & Quéré (2001), and Zhong *et al.* (2000). The most relevant, recent experimental investigation of mantle plumes has been carried out by: Davaille (1999), Davaille *et al.* (2002), Jellinek & Manga (2002, 2004) and Schaeffer & Manga (2001).

The similarities and differences of these previously published convection simulations with respect to the convection model developed in this study, will be discussed in detail in the following sections. One distinct and fundamentally important feature of our convection modelling is the ability to dynamically couple the surface plate motions to the buoyancy driven forces in the mantle. With the exception of Monnereau & Quéré (2001), previous investigations of time-dependent thermal convection in 3-D spherical geometry do not implement a dynamically consistent coupling of plates and mantle flow. As shown below, the coupling of the plates to the mantle convective flow is the key ingredient in understanding the evolution and stability of hotspot plumes.

Our first objective is this new analysis of plume dynamics in plate-coupled flows is to obtain an appropriate steady-state reference model which will serve as a starting point for the subsequent investigations of the time-dependent evolution of mantle heterogeneity when constant or changing surface plate configurations are imposed. This reference model must deliver realistic global observables associated with present-day terrestrial convection (as in Monnereau & Quéré 2001), which include surface heat flow, plate velocities and mantle potential temperature. This reference model is the basis for the following three tests of the impact of plates on convection with: (i) imposed no-net-rotation (NNR)-NUVEL-1 plate motions, (ii) imposed time-dependent plate velocities based on palaeomagnetic reconstructions of the past 120 Ma of plate tectonic evolution (Lithgow-Bertelloni & Richards 1998) and (iii) removal of the prescribed surface velocity constraints such that the plate motions evolve freely in response to buoyancy driven mantle flow. An important application of this final stage of modelling is to provide new insight into the dynamics of the present-day convection-induced rifting of the African continent.

The principal aim of this study is to develop the simplest, dynamically consistent model of 3-D spherical shell convection which is compatible with robust observational constraints. Although this model does not include a number of complexities, such as temperature-dependent viscosity or compositional heterogeneity, it captures the essential dynamics which allows us to elucidate the development and evolution of the most important features of terrestrial convection: linear mantle downwellings below subduction zones, passively divergent ridges, and especially focused hotspot plumes originating in the lower mantle. In contrast to past convection studies which have mainly considered the importance of subduction in mantle dynamics, this study will focus on the dynamics of hot upwellings in the mantle. In this regard, and in addition to satisfying fundamental global constraints, our convection model predicts distinct, isolated plumes, which we can correlate with a revised catalogue of 'primary' hotspots proposed in a recent study (Courtillot *et al.* 2003). The convection simulations presented below provide a simple and unified perspective on the dynamics of large-scale cold downwellings and hot upwelling plumes, both of which are intimately linked to the same plate-tectonic scale of mantle convection.

2 NUMERICAL CONVECTION FORMALISM

We employ a 3-D, spherical-shell, numerical model of time-dependent thermal convection in a mantle, which is treated as an incompressible viscous fluid. The dimensionless Boussinesq equations satisfying the principles of conservation of mass, momentum and energy are, respectively:

$$\boldsymbol{\nabla} \cdot \mathbf{v} = 0$$

$$-\boldsymbol{\nabla} P_d + Ra\, T\, \hat{\mathbf{r}} + \boldsymbol{\nabla} \cdot \boldsymbol{\tau} = 0$$

$$\partial T/\partial t + \mathbf{v} \cdot \boldsymbol{\nabla} T = \nabla^2 T + Q,$$

where $\mathbf{v}$ is the velocity vector, P_d is the dynamical pressure, T is the temperature field, $\boldsymbol{\tau}$ is the deviatoric stress tensor, Ra is the Rayleigh number, and Q is the dimensionless internal heating.

We non-dimensionalize the conservation equations according to the relations:

$$r = r/d,\ t = t\,\kappa/d^2,\ v = v\,d/\kappa \text{ and } T = (T - T_{\text{top}})/\triangle T,$$

with

$$\kappa = 6\ 10^{-7}\ \text{m}^2\,\text{s}^{-1},\ g = 10\ \text{m}\,\text{s}^{-2},\ \triangle T = 2000\ \text{K},$$

$$d = 2891 \times 10^3\ \text{m and } T_{\text{top}} = 0.$$

The Rayleigh number appearing in the above momentum conservation equation is defined as:

$$Ra = \frac{\alpha\ g\ d^3\ \rho\ \triangle T}{\kappa\ \eta}.$$

Owing to the assumption of incompressibility, the temperature at the CMB lies below the estimated range 2650 K (Boehler 1992) to 4000 K (Boehler 1996). The introduction of compressibility would add an adiabatic gradient to $\triangle T$ (Jeffreys 1930) and it should, therefore, be understood that the temperature increases predicted by an incompressible model are superadiabatic. Nevertheless, we found that the particular choice of a 2000 K (superadiabatic) increase across the mantle does not play a significant role in determining the pattern and amplitude of temperature heterogeneity in the convection solutions presented below.

In the upper mantle, the coefficient of thermal expansion $\alpha(r)$ is assumed to decrease linearly from a value of $3.5 \times 10^{-5}\,\mathrm{K}^{-1}$ at the surface to $2.5 \times 10^{-5}\,\mathrm{K}^{-1}$ at 670 km depth. Following Chopelas & Boehler (1992), we assume that the lower-mantle value of $\alpha(r)$ decreases from $2.5 \times 10^{-5}\,\mathrm{K}^{-1}$ at 670 km depth to $1.0 \times 10^{-5}\,\mathrm{K}^{-1}$ at the CMB.

The numerical solution of the momentum equation is carried out in both the spectral and spatial domains, in which the horizontal variation of the flow variables are expressed in terms of spherical harmonics (up to degree and order 90) and radial variations are solved by finite differences (with 100 radial nodes). The temperature equation is solved entirely in the spatial domain with finite differences, using an alternate direction inversion over a grid of 100 radial nodes, 180 longitudinal nodes and 90 latitudinal nodes.

The convection model includes a finite set of rigid tectonic plates which are dynamically coupled to the buoyancy induced mantle flow. All lithospheric plates in the model are assumed to be 90 km thick. The convection models presented below incorporate 14 plates whose geometry is given by the NUVEL-1 model (De Mets *et al.* 1990) in which we also include the geometry of the Somalia plate (Harper 1986).

The plates are coupled to the mantle using a torque balancing procedure which depends on the flow-induced viscous stresses generated by the internal mantle flow and the flow associated with the surface plates. This method neglects all of the plate boundary forces. The plates yield at zero stress at convergent boundaries and there is no friction along transform fault. In general, the magnitude of the predicted plate velocities would be reduced if plate boundary forces were included. This plate coupling theory, which was previously implemented in time-dependent spherical convection models by Monnereau & Quéré (2001), was first applied to instantaneous flow models in spherical geometry by Hager & O'Connell (1981) and subsequently extended by Ricard & Vigny (1989). The plate modelling approach is similar to that first used in Cartesian geometry by Gable *et al.* (1991) and later by Lowman *et al.* (2001).

In view of the fundamental role of the plate-coupling theory in the convection simulations presented here, a brief discussion of its importance is in order. To begin, it should be noted that we no longer require the traditional characterization of forces acting on the plates, as 'slab pull/suction', 'ridge push', 'mantle drag' used by Forsyth & Uyeda (1975) and Chapple & Tullis (1977). These early models of plate dynamics considered local force balances acting at plate boundaries and the connection to the underlying mantle flow was only parametrized in terms of a drag coefficient. The drag coefficient of any one plate was treated independently of that of the other plates. This simplified parametrization ignored that the motion of a plate was coupled to viscous stresses in the mantle that will also affect the motions of all other plates. Our plate-coupled convection formalism explicitly determines the viscous torques acting on the base of the plates and these driving forces are an integral of the buoyancy forces generated at all locations and at all depths in the mantle, not just at the surface. Indeed, we find that buoyancy forces generated at mid-mantle depths provide strong contributions to the plate driving torques and such deep-seated forces cannot be simply parametrized as 'slab pull' or 'ridge push'. The physical connection between mantle flow and plate motions is, therefore, much more complex than in the classical parametrized force models.

The plate-coupling procedure we employ shows that subducted slabs are efficient driving forces for the motions of Earth's tectonic plates. A plate dynamically linked to a subduction zone, as the Pacific plate will, therefore, have a much greater velocity than a plate surrounded by oceanic ridges, as the African plate. Indeed, we find (see below) that the motion of the African plate is driven by viscous stresses generated by remote subducted slab heterogeneity in the mantle.

We employ a NNR reference frame to model the surface plate motions. This reference frame is defined as having a zero dipolar (spherical harmonic degree 1) toroidal flow component. A degree-1 surface toroidal flow corresponds to the net rotation of the lithosphere and in a mantle with purely depth-dependent viscosity, the entire mantle rotates in unison, as a rigid body and will, therefore, have no associated shear stresses. Consequently, the degree-1 toroidal component of mantle flow will not provide any contribution to the torque balance acting on the tectonic plates and it is always set to zero in the convection models presented below, which are based on a spherically symmetric viscosity distribution.

An alternative reference frame for plate motions is provided by hotspots which have been assumed to be anchored to a stable or sluggish lower-mantle (Morgan 1971). Nevertheless, there are indications that the hotspots are subject to significant drift (Molnar & Stock 1987; Tarduno & Gee 1995) and the stability of the major hotspots is a matter of controversy (Norton 1995). In contrast to the NNR reference frame employed in our convection model, the present-day plate velocities in the (Pacific) hotspot reference frame show a clear westward rotation of the lithosphere, which is associated with a strong degree-1 toroidal component in the plate motions (Ricard *et al.* 1991; Gripp & Gordon 2002). This toroidal flow can be understood in terms of the dynamical effects of sublithospheric viscosity variations between oceans and continents of at least one order of magnitude (Cadek & Ricard 1992; Forte & Peltier 1994). The temperature, pressure and chemical dependence of viscosity is expected to produce a non-linear coupling of the poloidal and toroidal components (Forte & Peltier 1987, 1994) throughout the mantle. In the convection simulations presented below, however, this coupling will only occur in the lithospheric layer in which we define the tectonic plates.

3 REFERENCE CONVECTION MODEL

Our first objective is to establish a mantle convection model with dynamically coupled surface plates which also satisfies fundamental, globally averaged, geophysical observables. One such constraint is the mean value of the present-day tectonic plate velocities. On the basis of the NNR-NUVEL-1 model (Argus & Gordon 1991) (Fig. 1), the mean plate velocity is 3.85 cm yr^{-1}.

A second fundamental constraint is the average potential temperature under the plates and the corresponding mean surface heat flow (Stein 1995). In the Parsons & Sclater (1992) model the basal plate temperature is estimated to be 1350°C and in a more recent study (Stein & Stein 1992), it is estimated to be 1450°C.

It is more difficult to constrain the amplitude and source of the various contributions to the present-day global heat loss at the Earth's surface, which is estimated to be in the range 42 to 44 TW (Sclater

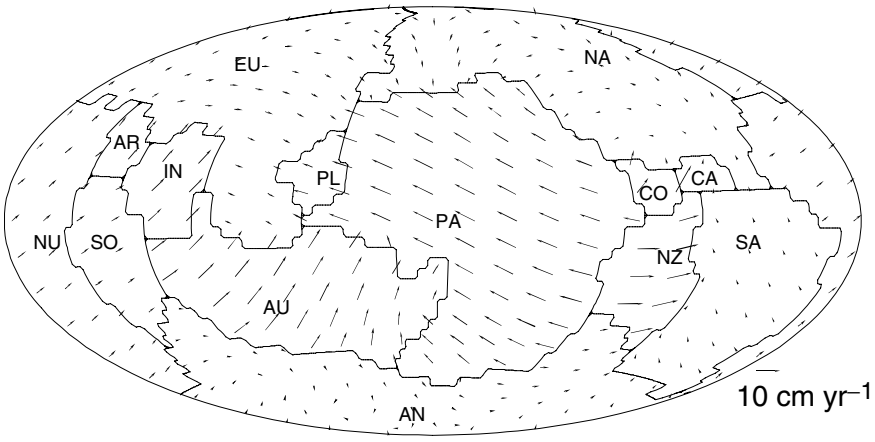

Figure 1. NUVEL-1 plate motions in the no-net-rotation (NNR) frame of reference. AN denotes Antarctica; AR, Arabia; AU, Australia; CA, Caribbean; CO, Cocos; EU, Eurasia; IN, India; NA, North America; NU, Nubia; NZ, Nazca; PA, Pacific; PL, Philippine; SA, South America and SO, Somalia.

et al. 1980; Pollack *et al.* 1993). The amount released by the crustal radioactive elements is assumed to be about 8 to 9 TW (Stacey & Loper 1988). We thus estimate that the total mantle and core contribution to surface heat flow should be between 33 and 36 TW. We assume that 20 TW of heating derives from distributed radioactive elements in the mantle (Stacey 1992) and that an additional 8 TW is provided by secular cooling of the mantle, assuming a minimal cooling rate of about 50 K Ga^{-1}. This cooling rate is consistent with constraints derived from petrological analyses of Archean MORB-like rocks (Abbott *et al.* 1994). The total mantle heat loss is thus assumed to be 28 TW, which is in the range of previous work (Monnereau & Quéré 2001).

The two model parameters which we vary to provide a fit to the mean surface observables (to within ± 10 per cent) are the mantle viscosity and the temperature at the CMB. We assumed for simplicity a two-layer mantle viscosity structure with a factor of 30 jump in viscosity at 670 km depth. This viscosity increase is suggested by previous geodynamically constrained mantle flow models which used the same two-layer parametrization (Hager 1984; Forte & Peltier 1987; Ricard & Vigny 1989).

We have thus explored the model space defined by the coordinate pair ($\eta_{\rm LM}$, $T_{\rm CMB}$), which, respectively, define the absolute lower-mantle viscosity and the CMB temperature. There is no guarantee, of course, that it is possible to fit three surface constraints by varying only two model parameters. We began with an initial convection model which was then adjusted by iteratively seeking values of $\eta_{\rm LM}$ and $T_{\rm CMB}$ which finally yielded the best overall fit to the mantle potential temperature, the mean surface plate velocities and the globally averaged heat flux. We were thus able to fit the global surface observables with $\eta_{\rm LM} = 25 \times 10^{21}$ Pa s and $T_{\rm CMB} = 2000^{\circ}$C. On the basis of these viscosity and temperature values, the reference model Rayleigh numbers $Ra_{\rm LM}$ (for the lower mantle) and $Ra_{\rm UM}$ (for the upper mantle) are, respectively, 2.2×10^6 and 1.3×10^8 and the equivalent Roberts (internal heating) Rayleigh numbers are $Ra^H_{\rm LM} = 8.6 \times 10^7$ and $Ra^H_{\rm UM} = 5.1 \times 10^9$. Using these input values, the reference convection model delivers the following globally averaged surface observables: 1) mean plate velocity is 3.57 cm yr^{-1}, 2) mantle potential temperature is 1223°C, and 3) global heat flow at top of mantle is 34.5 TW.

When the reference convection model reaches steady state, we observe stable flow and temperature fields (Fig. 2) which are characterized, in one hemisphere, by a nearly continuous, linear subduction zone and, in the opposite (Pacific) hemisphere, by a chain of four hotspot-like plumes which are located on the same great-circle arc.

The spherical convection simulations of Zhong *et al.* (2000) and Monnereau & Quéré (2001), which included a plate-like surface boundary condition, clearly show the production of focused hotspot-like thermal upwellings in models with and without temperature-dependent viscosity variations. We therefore conclude, on the basis of the present study, that the presence or absence of strongly focused, upwelling thermal plumes in 3-D spherical geometry is dependent on the particular choice of input model parameters, with the absolute mantle viscosity and internal heating rates likely being the most important control variables.

A whole-mantle cross-section of the temperature and flow fields (Fig. 2b) shows that the convective flow is essentially vertical below the subduction-zone boundary defined by the convergence of two plates. We also note that at this convergent boundary the fastest plate controls the flow dynamics below the subduction zone such that in the deep mantle, the cold return flow develops below the slowest plate.

Profiles of the radial velocity field (Fig. 3) show that the maximum value of the root-mean-square (rms) vertical flow $\langle u_r \rangle$, defined as $\langle u_r \rangle^2 = \frac{1}{4\pi} \int\int u_r(r, \theta, \phi)^2 \cos\theta \, d\theta \, d\phi$ ($\theta =$ latitude, $\phi =$ longitude) is 0.56 cm yr^{-1} (Fig. 3a). The maximum vertical velocity in the downwellings (Fig. 3b) is 11.7 cm yr^{-1} and it is attained in the mid-upper mantle. Conversely, the maximum vertical velocity in the upwellings is 7.4 cm yr^{-1} and it also is attained in the mid-upper mantle.

On the basis of the vertical flow profiles (Fig. 3b), the mean (vertically averaged) upwelling speed is 3.7 cm yr^{-1}, implying an estimated transit time of about 80 Ma for the hotspot-like upwellings across a steady-state mantle. Similarly, the mean downwelling speed is 5.8 cm yr^{-1}, which implies an estimated mantle transit time of about 50 Ma for the descent of subducted material. The rms vertical flow at 670 km depth (0.53 cm yr^{-1}) yields a lower-bound estimate of 277 Ma for the lower-mantle recycling time due to mass flux between the upper and lower mantle.

4 MODELLING CONVECTION WITH NUVEL-1 PLATE MOTIONS

Here we describe the impact of present-day plate motions on mantle convection dynamics. The basic approach we followed

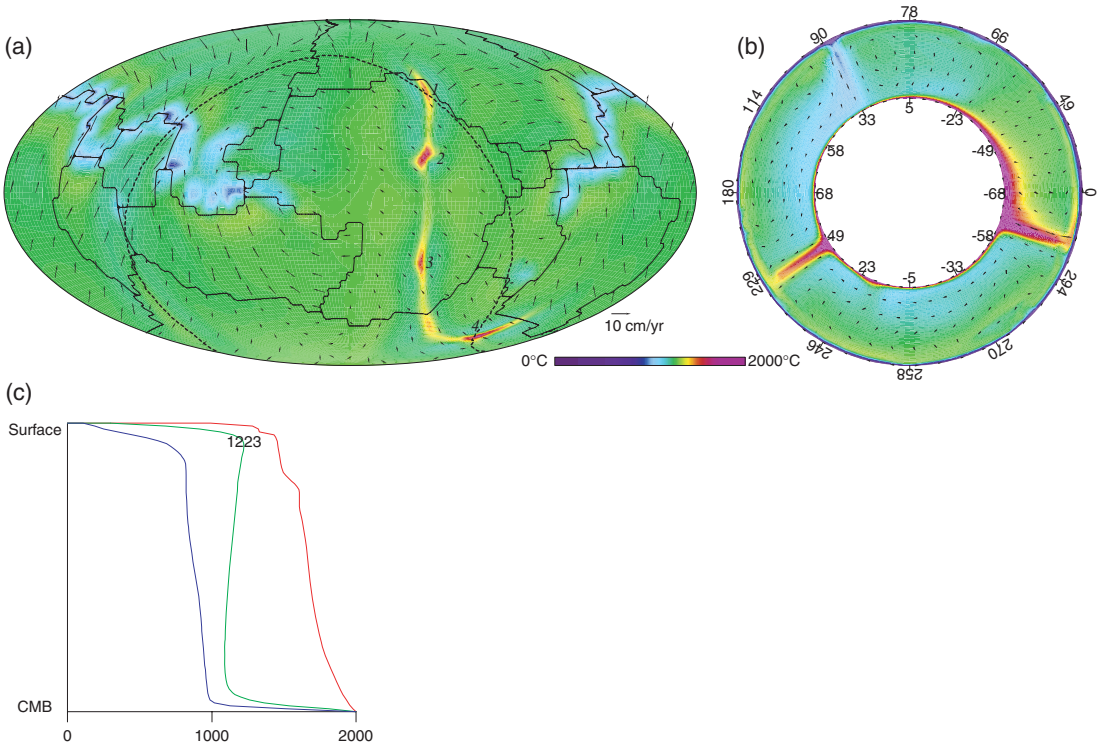

Figure 2. Thermal structure of the reference convection model. (a) The lateral temperature variations at 670 km depth. The predicted surface velocity field (black arrows) and surface plate boundaries (solid black lines) are superimposed. (b) Whole-mantle cross-section, along dashed line in (a), showing mantle temperature with the velocity field (black arrows) superimposed. Note that the sublithospheric velocity field below the subduction zone is vertical. (c) Radial temperature profiles showing the geotherm (green line), the hottest temperatures in mantle upwellings (red line), and the coldest temperatures in the downwellings (blue line).

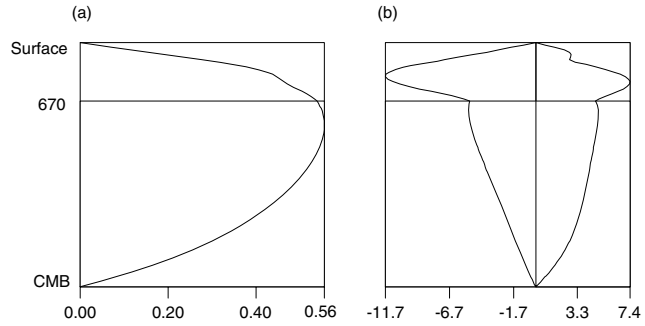

Figure 3. Flow velocities in the reference convection model. (a) Depth variation of the horizontally averaged (in a root-mean-square sense) radial velocity. (b) Radial velocity maxima in mantle downwellings (negative values) and upwellings (positive values). Units are cm yr^{-1}.

consists of using the radial profile of mean mantle temperature (the geotherm) from the reference convection model (described in the previous section) and prescribing the NNR-NUVEL-1 plate motions (Argus & Gordon 1991) as a surface boundary condition for our time-dependent convection model. In the convection simulations presented here, the NNR-NUVEL-1 velocity field is supplemented by an explicit description of the motion of the Somalia plate (Kreemer *et al.* 2003).

We note that the modelling procedure here is radically different from that employed in the reference convection model, discussed in the previous section. In the reference model we ensured that there is always a dynamical balance of the flow-induced torques acting on the surface plates (Ricard & Vigny 1989), whereas this constraint is no longer imposed when we employ a prescribed surface velocity field.

4.1 Model evolution prior to steady state

We define $t = 0$ as the initiation time for the convection simulation, which uses the prescribed NNR-NUVEL-1 surface plate motions and the mantle geotherm extracted from the reference convection model. Here we consider the predicted mantle thermal structure and flow field at a model time t, where $0 < t < t_{ss}$ and $t_{ss} \approx 550$–600 Ma denotes the time at which the model reaches steady state (Fig. 5e) . It is useful to consider the model results prior to steady-state conditions because mantle convection in the present-day Earth is not likely to be in a steady-state configuration, as evidenced by geologically 'recent' supercontinent break-up (Storey 1995), by continuous changes in the geometry and dynamics of the plates in the Cenozoic (Lithgow-Bertelloni & Richards 1998), and by the corresponding mantle hotspot motions (Steinberger & O'Connell 1998) and variations in subduction zone geometry.

In Fig. 4 we observe a snapshot of the convection model at model time $t = 310$ Ma, prior to achieving steady state. At this time the global heat flow at the top of the mantle is approximately 35 TW, which is essentially identical to the estimated value for the Earth, and the global heat flow crossing the CMB is 8 TW. The mantle potential temperature is $T = 1188$°C and the mean plate velocity (3.85 cm yr^{-1}) is of course given by the NNR-NUVEL-1 model.

The subduction zones are organized into a quasi-continuous line which also includes a triple branch at the junction of the Pacific, Australian and Eurasian plates (Fig. 4a). We explored the

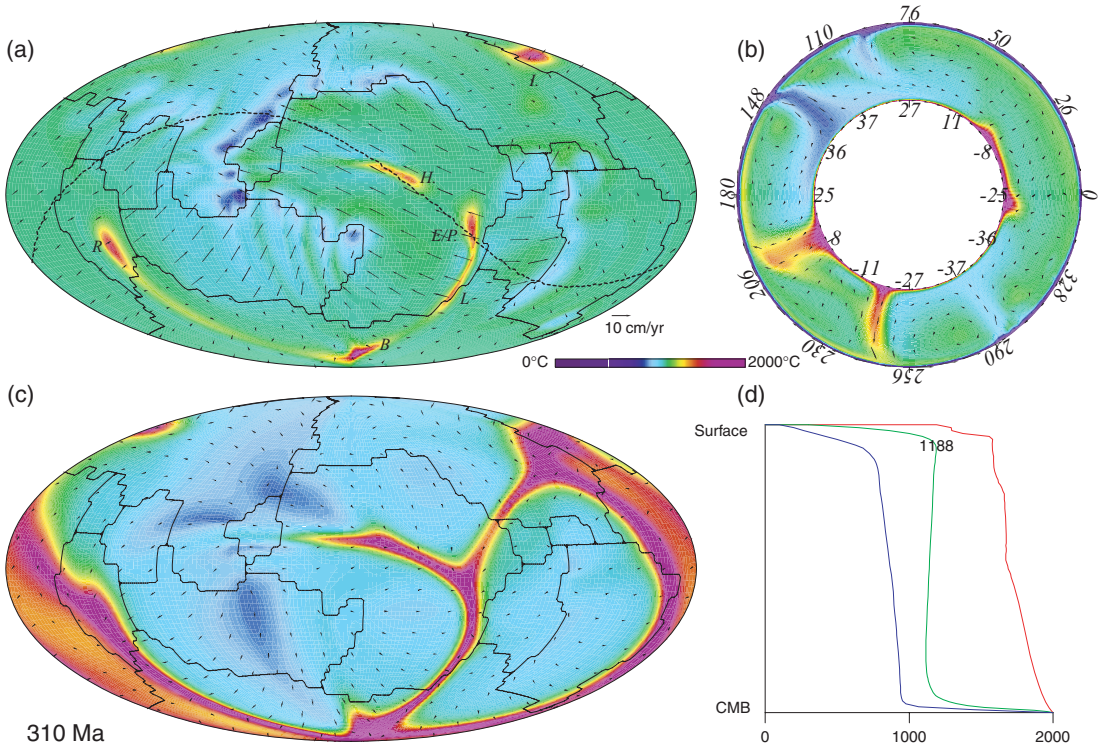

Figure 4. Convection model with prescribed NNR-NUVEL-1 surface plate motions at time $t = 310$ Ma. (a) The lateral temperature variations at 1500 km depth. The prescribed surface velocity field (black arrows) and surface plate boundaries (solid black lines) are superimposed. The six predicted 'hotspot'-like mantle plumes are labelled according to their associations with the primary plumes identified by Courtillot *et al.* (2003). H = Hawaii, E/P = Easter/Pitcairn, L = Louisville, B = Balleny, R = Réunion, and I = Iceland. (b) Whole-mantle cross-section, along dashed line in (a), showing mantle temperature with the velocity field (black arrows) superimposed. (c) The lateral temperature variations at 2690 km depth with the corresponding horizontal velocity field (black arrows) superimposed. (d) Radial temperature profiles showing the geotherm (green line), the hottest temperatures in mantle upwellings (red line), and the coldest temperatures in the downwellings (blue line).

time-dependent behaviour of the upwellings and downwellings (images not shown here) and we found that subducted material will take about 100 Ma to descend to the bottom of the mantle and, about 50 Ma later, hot plume material will begin to erupt from the lower thermal boundary layer at the CMB.

As in the case of the reference convection model, we again find that the fastest plate at a subduction zone will control the evolution of the downwelling flow below the convergent boundary. For example (Figs 4a–c), the main component of the return flow due to the subduction of the Pacific plate will be located under the Eurasian plate. We also note that the subduction due to the convergence of the Indian plate produces a dominant downward cold current below the Eurasian plate, but at greater depth the interaction with the return flow driven by the Pacific plate subduction will produce an apparent 'roll back' of the Indian downwelling. An alternative, tomography-based interpretation of the roll-over of deep subducting flow below India has been proposed in terms of the history of the closing of the Tethys ocean (van der Voo *et al.* 1999).

At the base of the mantle (Fig. 4c), we find a striking pattern of quasi-continuous, globe encircling, 'hotlines', one under the Pacific Ocean and two others located under the eastern and western boundary of the Nubia Plate. The junctions of these three hotlines, which appear to correspond to stagnation points in the horizontal flow field at the CMB, define the source regions for five focused cylindrical upwellings. One additional focused upwelling originates from the East Pacific hot line (Fig. 4c).

The position and the geometry of the hotlines appear to be controlled by the cold downwellings as they spread out along the CMB, such that the hotlines (and hence the cylindrical upwellings) are laterally displaced by about 60° from the centres of the downwellings (Fig. 4c). The impact of cold downwellings on the location and morphology of hot upwellings has also been observed in previous studies of 3-D spherical convection with plate-like surface conditions (Zhong *et al.* 2000; Monnereau & Quéré 2001) and in analog laboratory experiments (Gonnermann *et al.* 2004). Convection simulations with internal heating in 3-D Cartesian geometry have also shown a similar control of cold downwelling flow on upwelling plumes (Labrosse 2002). Since the cold downwellings control the position of the deep-mantle hotlines, the associated upwelling plumes (Fig. 4a) may arise either inter- or intraplate (i.e. appear to be independent of the surface plate configuration).

We have obtained six mantle upwellings (Fig. 4a) whose locations are very close to present-day hotspots on Earth's surface, most of them considered as being primary by Courtillot *et al.* (2003). The agreement between the locations of the upwelling plumes and the actual hotspots is of course not exact but the overall correspondence is quite good, especially considering that these upwellings are generated in a relatively simple theoretical convection model. Four of the focused upwelling plumes define isolated hotspots and appear to be located near the present-day locations of the Iceland, Hawaii, Réunion and Balleny hotspots. The hotspot-like plume, which we call 'Hawaii' is located in the middle of the deep-mantle return flow driven by cold downwellings which originate along the circum-Pacific subduction zones. The location of the two other upwelling plumes seem to correspond to the present-day locations of the Easter/Pitcairn and Louisville hotspots.

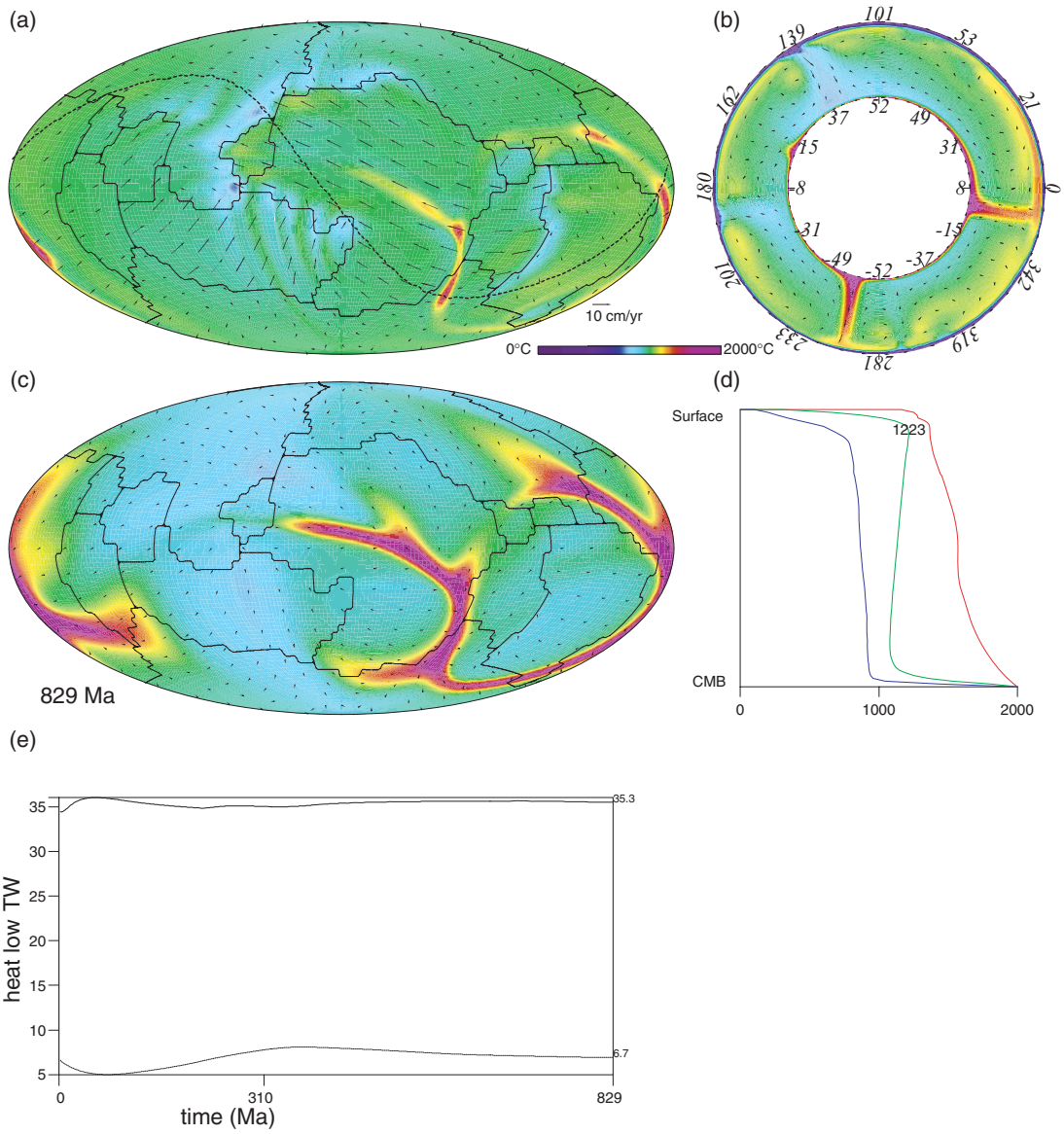

Figure 5. Convection model with prescribed NNR-NUVEL-1 surface plate motions at time $t = 829$ Ma (steady state). (a) The lateral temperature variations at 1500 km depth. The prescribed surface velocity field (black arrows) and surface plate boundaries (solid black lines) are superimposed. The number of 'hotspot'-like thermal plumes (4) is the same as in the reference model (Fig. 2). (b) Whole-mantle cross-section, along dashed line in (a), showing mantle temperature with the velocity field (black arrows) superimposed. Note the elongation of the plume head by the surface plate movement. (c) The lateral temperature variations at 2690 km depth with the corresponding horizontal velocity field (black arrows) superimposed. (d) Radial temperature profiles showing the geotherm (green line), the hottest temperatures in mantle upwellings (red line), and the coldest temperatures in the downwellings (blue line). (e) Time evolution of heat flow at the surface and at the core–mantle boundary (CMB) for the convection model with prescribed NNR-NUVEL-1 surface plate motions. We note that at $t = 310$ Ma, steady state conditions have not been achieved.

It is interesting to note that the six 'hotspot-like' thermal plumes in our convection model is very close to the number of major hotspots which Courtillot *et al.* (2003) have identified for the Earth. The focused upwelling plumes (Fig. 4a), which we have associated with the Easter, Hawaii, Louisville, Réunion and Iceland hotspots have also been identified as being 'primary' hotspots, according to the criteria adopted by Courtillot *et al.* (2003). It is also noteworthy that many of the 49 hotspot candidates considered by Courtillot *et al.* (2003) are localized above the two lower-mantle hot lines that extend beneath the African continent (Fig. 4c).

4.2 Model at steady state

The convection simulation yields a steady-state thermal structure at $t \approx 550$–600 Ma (Fig. 5e). We find that well into the steady-state regime, at time $t = 829$ Ma, the temperature variations in the deep mantle (Fig. 5c) are controlled by cold downwellings which have spread out over the CMB, thereby sweeping aside the hotlines which are now located far from the downwelling centres. In particular, the two formerly separate hotlines below the Nubian plate (Fig. 4c) have now been swept into a single structure located directly below the surface location of the African continent (Fig. 5c).

The number of hotspot-like thermal plumes has decreased to four (Fig. 5a), the same number as in the reference convection model, and the location of these upwellings (Fig. 5b) remains nearly stationary throughout the steady-state regime. From Figs 5(a) and (c) we note that the hot upwellings are again focused above triple-point intersections of the deep-mantle hotlines. The stationary and vertical character of the upwelling plumes (Fig. 5b), which differs from the time-dependence observed by Labrosse (2002), may be explained in terms of the large viscosity increase between upper and lower mantle, also by the 3-D spherical geometry that effectively acts as a viscosity increase (Jarvis 1993), and by the stabilizing role of the surface plates, which control the geometry of the mantle downwellings. The stability of the upwelling plumes is dependent on the stability of the deep-mantle hotlines which is, in turn, controlled by the dynamics of the cold downwellings.

The oblique near-surface trajectory (Figs 4b and 5b) of the cold downwellings (the 'subduction zones'), is quite different from the symmetric geometry in the reference model (Fig. 2b). The obliqueness of the 'western Pacific' subduction zone is due to the rapid convergence of the Pacific plate, such that the associated near-surface flow thrusts below the Eurasian plate. This asymmetry of the surface downwellings, due to the imposed surface plate velocities, determines the geometry of the cold return flow in the deep mantle and hence the location and number of hot upwelling plumes. We also note that, prior to steady state, this 'forced subduction' effect yields a sublithospheric mean mantle temperature (Fig. 6a), which is colder than that in the reference model or at steady-state conditions (Fig. 6b).

At steady state, the mantle heat flow (35.3 TW, Fig. 5e), the average plate velocity (3.85 cm yr^{-1}) and the temperature under the upper thermal boundary layer (1216°C) are close to those obtained in the reference convection model (34.5 TW, 3.57 cm yr^{-1}, 1223°C), in which the NNR-NUVEL-1 plate motions were not prescribed. We do not, of course, expect exactly the same values since the dynamical treatment of the plates is different in the two models. Nonetheless, the good agreement demonstrates the excellent compatibility between the mantle thermal structure in the reference model and the present-day plate velocity field.

4.3 Comparison with seismic tomography

As we have seen, cold downwellings in the deep mantle play a key role in controlling the configuration of the hotlines and hence in determining the location and the number of the principal upwelling plumes (see also Labrosse 2002). In view of the importance of deep-mantle thermal structure for understanding plume dynamics, it is useful to consider whether the convection simulations presented above bear any resemblance to the present-day structure of the lowermost mantle as inferred by seismic tomography.

Any comparisons with seismic tomography are subject to considerable uncertainty arising from a wide variety of sources. These uncertainties include, for example, the question of the resolution of deep-mantle structure provided by current seismic data coverage. There are also many questions related to the numerous simplifications and assumptions employed in our convection models, such as the neglect of temperature-dependent rheology, which is not resolved in our convection code or the neglect of compositional heterogeneity. These uncertainties must be borne in mind when evaluating the comparison we present here. We first note that the average amplitude of the lateral temperature variations near the CMB is approximately 500°C (Fig. 5c) and this is close to that which has already been inferred in a recent joint seismic-geodynamic investigation of deep-mantle heterogeneity (Forte & Mitrovica 2001). If we assume that thermal heterogeneity is the dominant source of seismic shear velocity anomalies and we further assume a temperature derivative of $d \ln V_s/dT = -7 \times 10^{-5}$ K^{-1} in the lowermost mantle (Forte & Mitrovica 2001), we may translate the temperature variations in the convection model into equivalent seismic anomalies.

In Fig. 7, we directly compare the lateral temperature variations in the lowermost mantle predicted by the steady-state convection model with the equivalent temperature anomalies extracted from the Grand (2002) tomography model. There is a broad agreement between the location and elongation of the hotlines in the convection model and the similarly configured regions of hotter than average mantle in the tomography model. The match with the pattern of accumulated subducted heterogeneity below the western Pacific is also good. It is also important to note that the absolute amplitude of the temperature heterogeneity in the convection model is in excellent agreement with that derived from the tomography model. This result constitutes an important independent verification of the consistency and plausibility of the temperature structure predicted by the convection model.

In view of the agreement between the amplitude and large-scale configuration of lateral temperature variations at the base of the mantle inferred from seismic tomography and those predicted by the convection model, it is worth considering the implications from the perspective of heat flow across the CMB. The lateral variations in CMB heat flow maintained by mantle convection may have a significant modulating effect on the activity of the core geodynamo, especially on the dynamics of geomagnetic polarity reversals (Glatzmaier *et al.* 1999).

We find that the lateral variations in CMB heat flux are almost perfectly anticorrelated with the lateral temperature variations in the lower thermal boundary layer (Fig. 5c), as would be expected for an isothermal boundary condition. The mean heat flux across the CMB for steady-state convection (Fig. 5e) is about 45 mW m^{-2}, equivalent to a total CMB flux of about 7 TW. The latter value is close to the values proposed in recent core evolution models, which invoke the presence of radioactive potassium in the core (Nimmo *et al.* 2004). We find that the maximum heat flux, at the centres of cold downwellings below the western Pacific, is about 140 mW m^{-2}, whereas the minimum heat flux, at the centres of hot upwelling below the Pacific and below Africa is nearly zero. Such lateral variations in CMB heat flux may have an important impact on geomagnetic reversals (Glatzmaier *et al.* 1999).

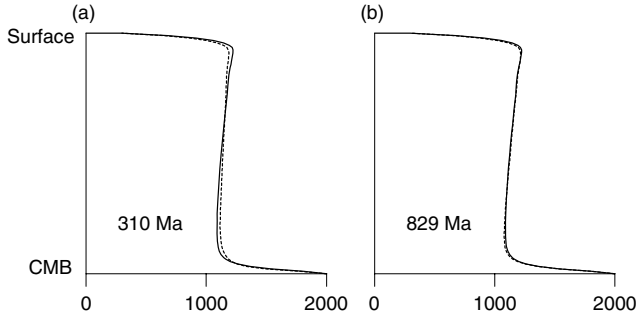

Figure 6. Mantle geotherms for the reference model (solid lines) and the model with prescribed NNR-NUVEL-1 plate motions (dashed lines). (a) Comparison at time $t = 310$ Ma, and (b) at time $t = 829$ Ma. At steady state (in b), the two geotherms are almost identical.

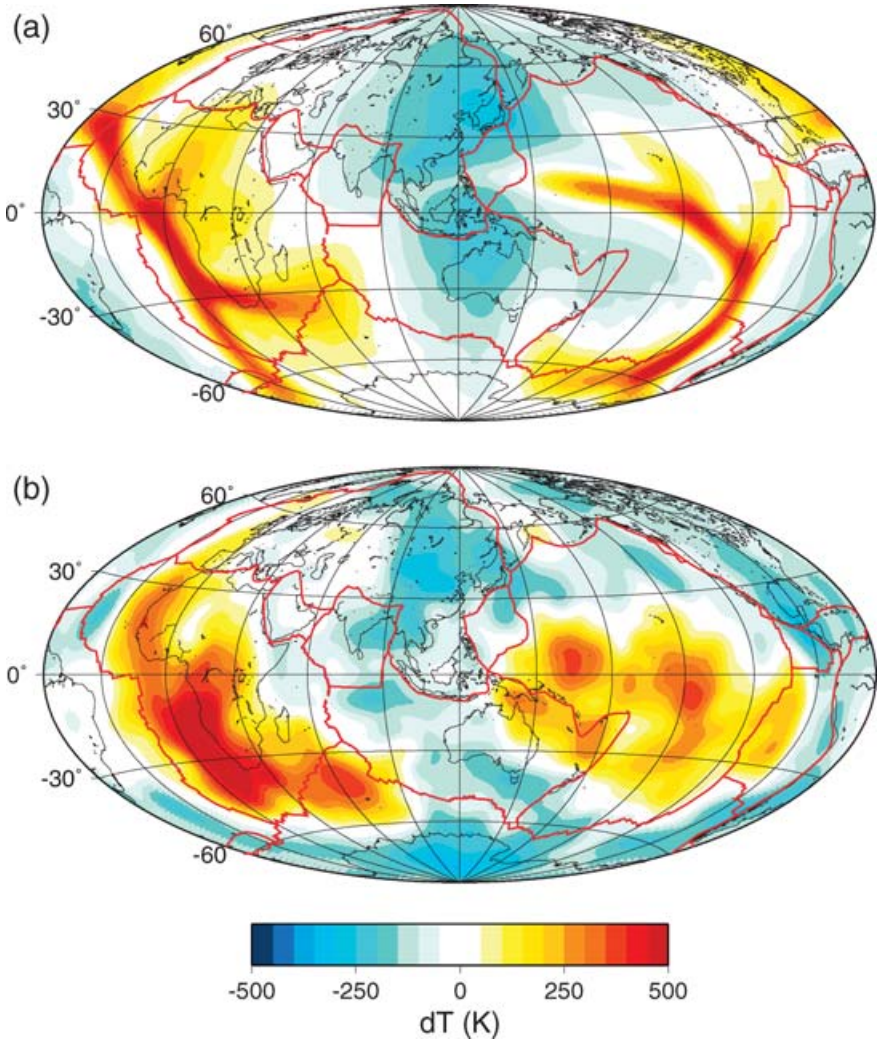

Figure 7. Comparison of deep-mantle heterogeneity derived from seismic tomography and from the convection model. (a) Vertical average of the temperature anomalies in the depth range 2650 to 2891 km obtained from the convection model in Fig. 5(c). (b) Equivalent temperature anomalies in the same depth range obtained from seismic shear velocity anomalies in the Grand (2002) tomography model. The seismic anomalies are converted to temperature assuming a thermal derivative of $d \ln V_s / d T = -7 \times 10^{-5}$ K^{-1} (see text for details). The fields in both (a) and (b) have been synthesized from a spherical harmonic expansion up to degree and order 32.

The reconstruction of tomographically inferred mantle heterogeneity at the base of the mantle, using a numerical convection model (as in Fig. 7), has also been considered by Bunge *et al.* (2002). These authors suggest that a time interval between 150 and 200 Ma is required for subducted slabs to reach the CMB and, therefore, it is not possible to obtain a good representation of heterogeneity in the deepest mantle using convection models that integrate tectonic plate motions, which encompass only the past 120 Ma of plate history. Our results suggest that by considering a simple convection model, which attains steady state under NNR-NUVEL-1 plate motions, or alternatively with a time-dependent plate motion history (see below), it is possible to obtain a broad agreement with the temperature heterogeneity derived from seismic tomography. Clearly there are a number factors, which must be properly accounted for, and these include the relative fraction of bottom and internal heating, the assumed viscosity structure, the reference frame in which the plate motion history is reconstructed, and the length of time over which the convection simulations are iterated forward.

5 CONVECTION WITH TIME-DEPENDENT PLATE HISTORIES

It is important to asses the robustness of our convection results, particularly with regard to the dynamics and configuration of hot mantle upwellings. To this end, we carried out two complementary convection simulations incorporating the past 120 Ma history of tectonic plate evolution (Lithgow-Bertelloni & Richards 1998), a time period for which reliable reconstructions of the plate-motions are possible. We first considered a convection simulation which was initiated with the temperature structure in the reference convection model discussed above. As the upper-mantle viscosity value ($\eta_{\rm UM} = 8.3 \times 10^{20}$) is somewhat larger than estimates derived from joint inversions of convection and post-glacial rebound data

(Mitrovica & Forte 2004), we ran a second experiment with a revised, geodynamically constrained estimate of viscosity.

5.1 Impact of plate-motion history on the reference model

Our first test involves a time-dependent simulation that starts with the 3-D temperature structure obtained by running a calculation with the reference-model geotherm and prescribed plate motions for the period [−119 Ma, −100 Ma] until steady state is achieved. This Mid-Cretaceous (−119 Ma) plate velocity field is the oldest estimate that can be reliably derived from palaeomagnetic reconstructions and hence our steady-state convection model for this period is the best initial condition we can obtain. It is obvious that this assumed starting model cannot incorporate any temperature evolution in the mantle for time periods earlier than −119 Ma and this constitutes an important source of uncertainty in the predictions we will present here. As already pointed out in Bunge *et al.* (2002), there are additional uncertainties in the palaeomagnetic plate reconstructions themselves, especially in the case of plates which have completely or nearly completely subducted (Izanagi, Phoenix, Kula, Farallon). It should, therefore, be recognized that the configuration of the subduction zones in the reconstructions are subject to considerable uncertainties.

The convection simulation was iterated forward from $t = -119$ Ma through all successive Mesozoic and Cenozoic stages of plate motion history. At $t = 0$ (present day) the simulation was then iterated forward with prescribed NNR-NUVEL-1 plate motions until $t = +710$ Ma, so that the entire span of the simulation is equal to the 829 Ma time interval explored in the NUVEL-1 convection model discussed in the preceding section. We note that at the beginning of the simulation, at $t = -100$ Ma, there are five identifiable hotspot plumes emanating from the top of the deep-mantle hotlines (see Fig. 8a). Remarkably, during the entire interval [−119 Ma, 0 Ma], the hotlines at the base of the mantle shift laterally by only small amounts and consequently the locations of the hotspot plumes are relatively stable (Figs 8 and 9). Extending the calculation a further 191 Ma into the future shows that the configuration of the lower-mantle hotlines is very similar to that in the NNR-NUVEL-1 convection model at $t = 310$ Ma, with a Y-shaped junction of hotlines under the eastern Pacific and a doublet of hotlines under the Nubia–Somalia plates (compare Figs 9d and 4c). The locations of both hotlines and hotspots in the preceding and present convection experiments are very similar to each other (compare Figs 8–9e, 5a and c), even though steady state has not yet been attained by the current simulation with the time-dependent plate configurations.

The key result is that, from start to finish, the convection simulation which incorporated the entire 120 Ma span of plate motion history yields nearly stationary hotlines at the base of the mantle. This result is due to the rather stable, large-scale 'horseshoe' pattern of circum-Pacific subduction which existed over the past 120 Ma, thereby focusing one hotline inside the horseshoe (under the central Pacific) and the other hotline outside

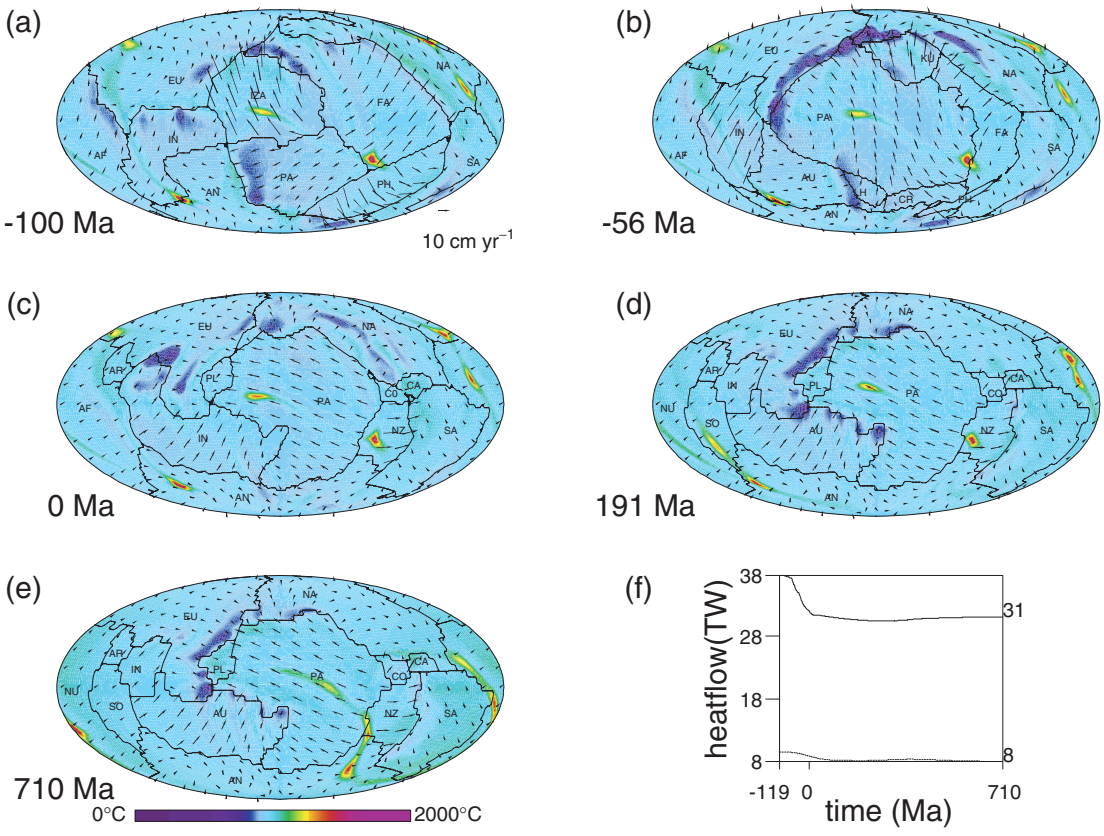

Figure 8. Lateral temperature variations at 1500 km depth for the reference convection model with plate-motion history for Mesozoic, Cenozoic and NNR-NUVEL-1 plate stages. The surface velocity field and surface plate boundaries are shown for the intervals: (a) −119 to −100 Ma. (b) −64 to −56 Ma. (c) −10 to 0 Ma. (d) 0 to 191 Ma. (e) 191 to 710 Ma. (f) Time evolution of heat flow at the surface and at the CMB for the reference convection model spanning 829 Ma of plate tectonic evolution. AF denotes Africa; AN, Antarctica; AR, Arabia; AU, Australia; CA, Caribbean; CO, Cocos; CR, Chatham Rise; EU, Eurasia; FA, Farallon; IN, India; KU, Kula; LH, Lhasa; NA, North America; NZ, Nazca; PA, Pacific; PL, Philippine; PH, Phoenix and SA, South America.

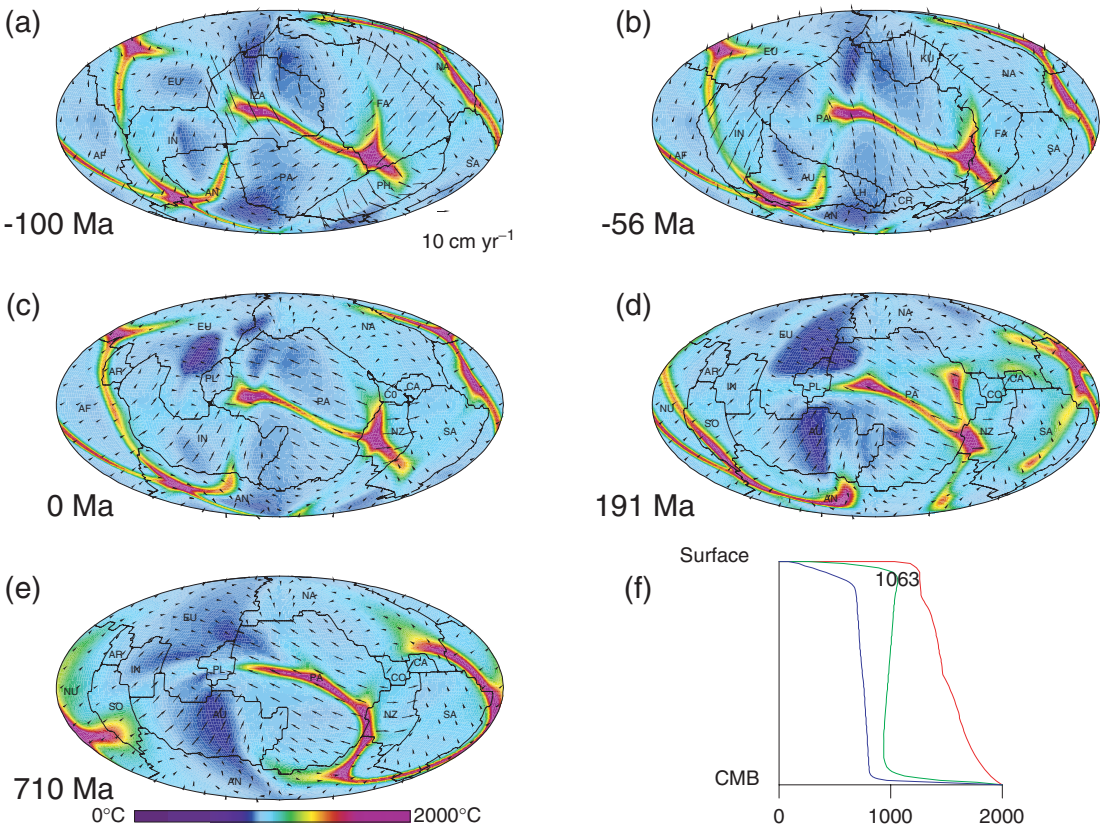

Figure 9. Lateral temperature variations at 2690 km depth for the reference convection model with plate-motion histories for Mesozoic, Cenozoic and NNR-NUVEL-1 plate stages. The surface velocity field and surface plate boundaries are shown for the intervals: (a) −119 to −100 Ma.(b) −64 to −56 Ma. (c) −10 to 0 Ma. (d) 0 to 191 Ma. (e) 191 to 710 Ma. (f) Radial temperature profiles showing the geotherm (green line), the hottest temperatures in mantle upwellings (red line), and the coldest temperatures in the downwellings (blue line). AF denotes Africa; AN, Antarctica; AR, Arabia; AU, Australia; CA, Caribbean; CO, Cocos; CR, Chatham Rise; EU, Eurasia; FA, Farallon; IN, India; KU, Kula; LH, Lhasa; NA, North America; NZ, Nazca; PA, Pacific; PL, Philippine; PH, Phoenix and SA, South America.

(under Africa). Since the predicted configuration of the hotlines for the stage [−119 Ma, −100 Ma] is under the future locations of the Pacific and African plates, in agreement with the configuration obtained by running a calculation with the present-day NNR-NUVEL-1 plate motions, it is readily understood why the present-day plate motions provide a sufficient surface boundary condition for modelling the generation of the principal, present-day hotspot plumes.

5.2 Impact of plate-motion history with a geophysically constrained viscosity profile

We next carried out a simulation in which we incorporate the palaeomagnetic reconstruction of surface plate evolution in a convection model which also includes geodynamically constrained values for mantle viscosity. We employ a two-layer viscosity model determined by averaging the absolute upper- and lower-mantle viscosities recently inferred in a joint inversion of convection and glacial isostatic adjustment data (Mitrovica & Forte 2004). In this new viscosity profile, $\eta_{\rm LM} = 12.4 \times 10^{21}$ Pa s and $\eta_{\rm UM} = 3.3 \times 10^{20}$ Pa s. The CMB temperature (2750°C) and internal heating (20 TW) have been changed to yield global predictions (mantle heat flow, mean plate velocity, potential temperature) that were within ±30 per cent of the observed values. This new reference model with freely moving plates delivers the following global surface observables: mean plate velocity is 5.01 cm yr^{-1}, mantle potential temperature is 1052°C, and surface heat flow is 36 TW. Following Coltice & Ricard (1999), we assumed that a part of the internal heating may be concentrated in a 300-km-thick D″ layer at the base of the mantle, to simulate the effects of a distinct, compositionally enriched thermal boundary layer. In contrast to the models discussed so far, we placed 12 TW of radiogenic heating in D″ and distributed the remaining 8 TW, which simulate the secular cooling, throughout the mantle. We found that this concentration of heat producing elements had the effect of increasing the propensity for hotspot plume generation compared to a model in which all heat sources were uniformly distributed in the mantle.

A new starting model was obtained on the basis of the new reference model geotherm by introducing the reconstructed plate velocities for the stage [−119 Ma, −100 Ma] and iterating to a steady state. As in the previous experiment, this starting model was subsequently run forward in time, incorporating the entire plate history for [−119 Ma, 0], and then iterated further to $t = +710$ Ma. We again find that the location and pattern of deep-mantle hotlines and associated hotspot plumes are very similar to those obtained in the preceding experiment (compare Figs 10, 11, 8 and 9). We note, however, that the radiogenically enriched D″ layer yields fluctuations in the heat flux across the CMB (Fig. 10f) that are greater than in the previous models.

It is, therefore, clear that a convection model with geophysically constrained values of mantle viscosity yields a pattern of plumes and deep-mantle heterogeneity, which is very similar to that

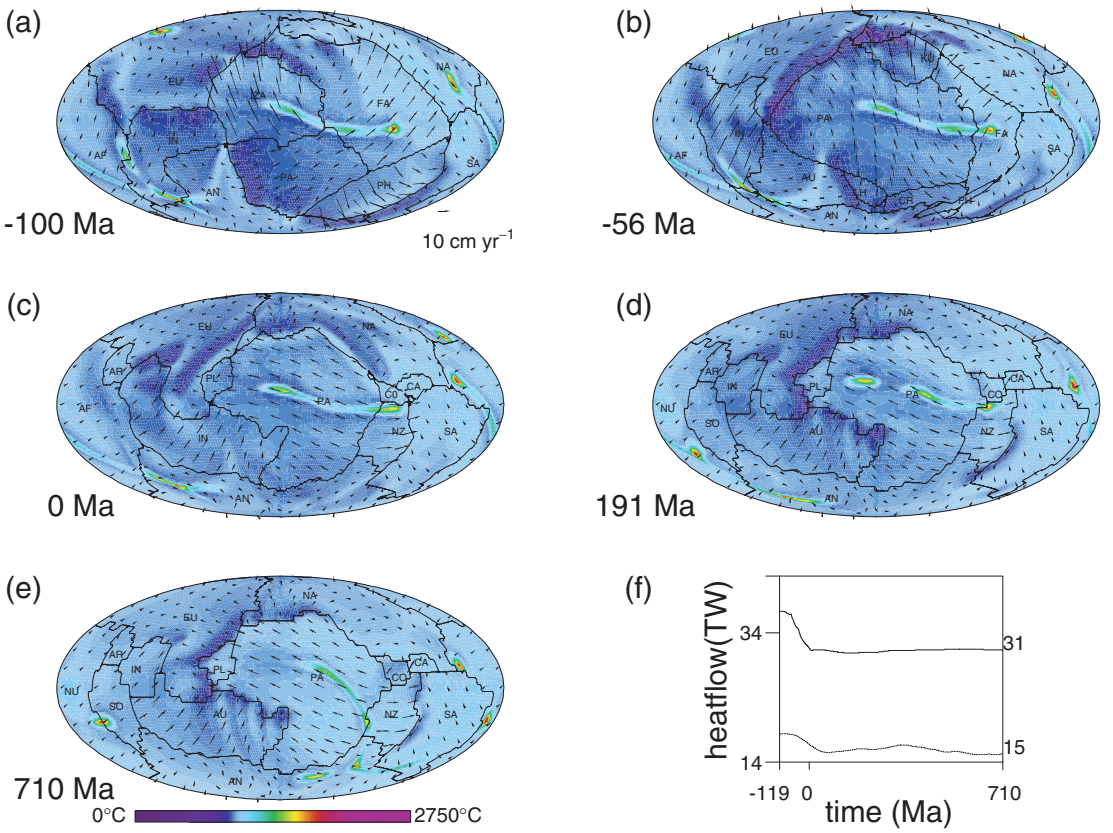

Figure 10. Lateral temperature variations at 1500 km depth for the convection model incorporating geodynamically constrained mantle viscosity and plate-motion histories for Mesozoic, Cenozoic and NNR-NUVEL-1 plate stages. The surface velocity field and surface plate boundaries are shown for the intervals: (a) −119 to −100 Ma. (b) −64 to −56 Ma. (c) −25 to −10 Ma. (d) 0 to 191 Ma. (e) 191 to 710 Ma. (f) Time evolution of heat flow at the surface and at the CMB for the reference convection model with plates-motion history spanning 829 Ma of plate tectonic evolution. AF denotes Africa; AN, Antarctica; AR, Arabia; AU, Australia; CA, Caribbean; CO, Cocos; CR, Chatham Rise; EU, Eurasia; FA, Farallon; IN, India; KU, Kula; LH, Lhasa; NA, North America; NZ, Nazca; PA, Pacific; PL, Philippine; PH, Phoenix and SA, South America.

obtained previously with the steady-state NNR-NUVEL-1 model. Although the input parameters for the two models are quite distinct, both models are required to satisfy the same present-day global constraints and both ultimately yield the same stable pattern of hotlines in the deep mantle. This experiment demonstrates the existence of several convection models, characterized by different input parameter values, which yield the same mantle structures provided that in each case we satisfy the fundamental globally averaged surface constraints.

6 MODEL EVOLUTION WITH FREE SURFACE PLATE MOTIONS

In the previous sections we considered the evolution of the mantle thermal structure subject to a 120 Ma history of Mesozoic–Cenozoic plate velocities followed by prescribed NNR-NUVEL-1 plate motions. Here we will explore the consequences of releasing the imposed plate velocities and allowing the plates to move freely in response to the buoyancy driven flow in the mantle.

6.1 Impact of free plate motions

We return to the convection simulation illustrated in Fig. 5 and now consider the dynamical evolution following the removal of the NNR-NUVEL-1 velocity constraint at model time $t = 829$ Ma. Since the surface velocities are no longer imposed, the plate motions are found to be largely directed by the buoyancy forces below subduction zones. The motion of the Pacific plate, in particular, is now characterized by a more symmetrical pattern of convergence along the circum-Pacific trench system and this implies an increase in the velocities of the Eurasian and North American plates, which must balance the material flux entering the subduction zones (Fig. 12a). By the same reasoning, we note that the South American plate motion shifts towards the Pacific subduction zone (Fig. 12a), as it would in the hotspot reference frame, rather than moving northwards as in the NNR reference frame (Fig. 4a). Overall, however, the global plate velocity field has changed little after releasing the imposed plate motions.

After allowing the model with free plate motions to run a further 20 Ma, we find that the configuration of the converging and diverging plate boundaries, and the locations of the upwelling plumes remain almost exactly the same (Fig. 12). When we ran the same experiment, allowing free plate motions at $t = 310$ Ma, we found that after a similar 20 Ma interval, the focused upwellings are subject to much greater change, in response to the large-scale internal flow.

The introduction of free plate motions, at $t = 829$ Ma, occurs at a time when the mantle thermal structure is in steady state and is compatible with the surface-plate motions. It is important to note that this compatibility is now occurring in a regime where the dynamical coupling of the plates to the buoyancy forces in the mantle is

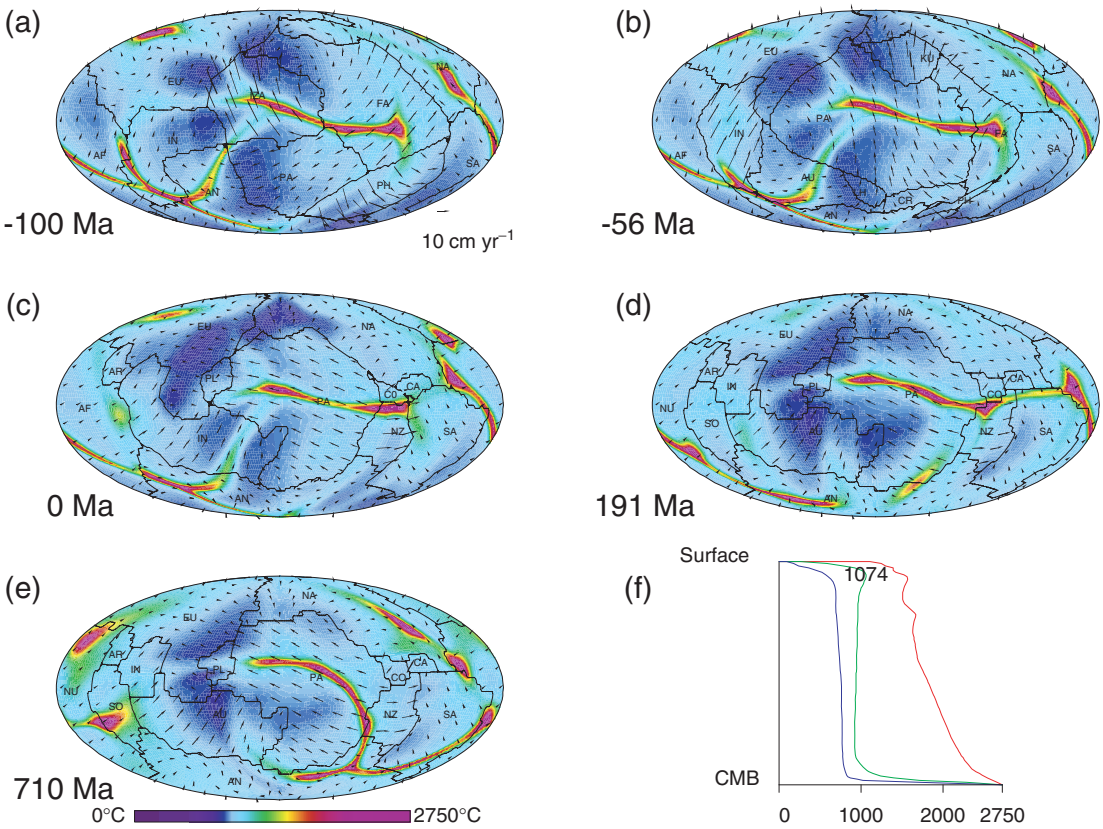

Figure 11. Lateral temperature variations at 2690 km depth for the convection model incorporating geodynamically constrained mantle viscosity and plate-motion histories for Mesozoic, Cenozoic and NNR-NUVEL-1 plate stages. The surface velocity field and surface plate boundaries are shown for the intervals: (a) −119 to −100 Ma. (b) −64 to −56 Ma. (c) −10 to 0 Ma. (d) 0 to 191 Ma. (e) 191 to 710 Ma. (f) Radial temperature profiles showing the geotherm (green line), the hottest temperatures in mantle upwellings (red line), and the coldest temperatures in the downwellings (blue line). AF denotes Africa; AN, Antarctica; AR, Arabia; AU, Australia; CA, Caribbean; CO, Cocos; CR, Chatham Rise; EU, Eurasia; FA, Farallon; IN, India; KU, Kula; LH, Lhasa; NA, North America; NZ, Nazca; PA, Pacific; PL, Philippine; PH, Phoenix and SA, South America.

perfectly balanced. In this stable regime the horizontal motion of the focused upwellings ('hotspot'-like plumes) is very small. The surface heat flow (35.2 TW), the average plate velocity (3.73 cm yr^{-1}) and the potential temperature under the lithosphere (1217°C) are all very similar to the values we found for the reference convection model.

6.2 Implications for African rift dynamics

An important consequence of releasing the imposed NUVEL-1 plate velocities is the predicted rifting of Africa along the Nubia–Somalia plate boundary (Fig. 12a). Prior to model time $t = 829$ Ma, the prescribed NNR-NUVEL-1 plate velocities include a Somalia rotation vector which was slightly different from the Nubia plate. We, therefore, ran a test simulation where the Nubia and Somalia plates had identical rotation vectors for $t < 829$ Ma and we again find, after allowing free surface plate motions at $t = 829$ Ma, that opening occurs along the Nubia–Somalia boundary.

This rifting occurs as a natural consequence of the mechanical coupling of the large-scale mantle flow under the Nubia and Somalia plates and does not appear to require the presence of a hot sublithospheric plume directly underneath the rift. In this regard, we note that at $t = 829.2$ Ma, the lower-mantle hotline has passed beneath the surface location of the Nubia–Somalia boundary and the main cause for the predicted rifting of Africa is the associated large scale upwelling. We recognize that the Afar hotspot is located nearby, at the triple junction of the Somalia–Nubia–Arabia plates, and the timing and relationship of rifting to the arrival of this hotspot plume is an open issue (e.g. Furman *et al.* 2004). Our model results suggest that the African rifting and the arrival of the Afar hotspot may be essentially simultaneous events whose common origin is the large-scale upwelling below the continent.

The opening along the East African rift has been related to large-scale extensional stresses which appear to characterize most of the African plate and this has been interpreted as inconsistent with the stress regime, which would be predicted on the basis of the ridge system which nearly encircles the African plate (Zoback *et al.* 1989). A proposed resolution for this apparent inconsistency involves the dynamical effect of a mantle upwelling below Africa (Zoback *et al.* 1989). Such an upwelling has also been invoked as an explanation for time-dependent uplift of southern Africa (Gurnis *et al.* 2000) and also to explain a number of global geodynamic constraints (Forte & Mitrovica 2001). The present convection simulation suggests that the opening of the African rift, which is driven by large-scale flow in the mantle, extends almost along the entire length of the Nubia–Somalia boundary and that this rate is greater than that observed by the NNR-GSRM-1 model (Kreemer *et al.* 2003).

The extensive volcanic activity along the African rift system has been attributed to the impact of numerous individual hot mantle plumes erupting from a very large-scale upwelling or convection

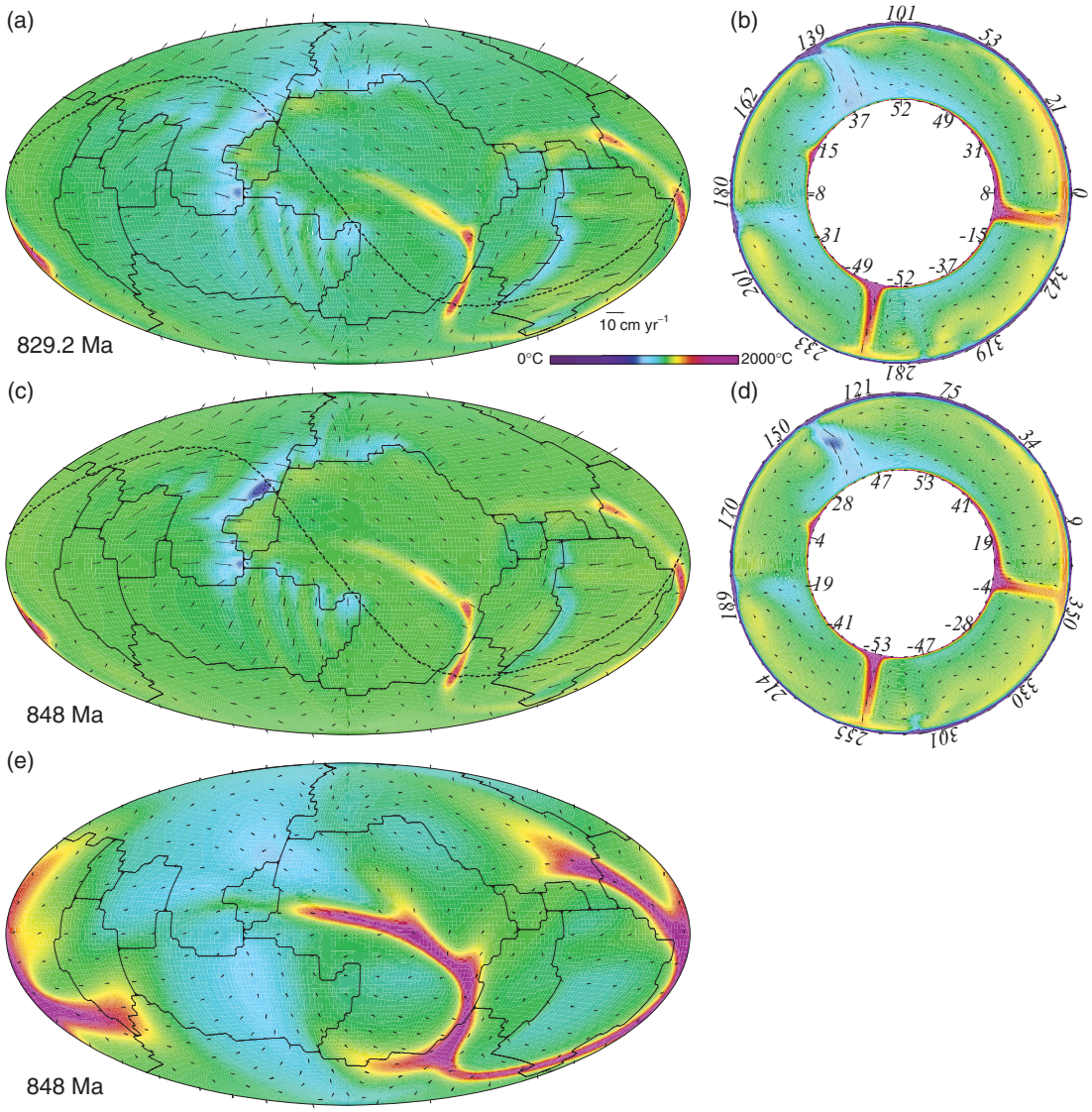

Figure 12. Convection model with free plate motions, following the release of the prescribed NNR-NUVEL-1 plate velocities. (a) The lateral temperature variations at time $t = 829.2$ Ma at 1500 km depth. The predicted surface velocity field (black arrows) and surface plate boundaries (solid black lines) are superimposed. (b) Whole-mantle cross-section, along dashed line in (a), showing mantle temperature with the velocity field (black arrows) superimposed. (c) The lateral temperature variations at time $t = 848$ Ma at 1500 km depth. The predicted surface velocity (black arrows) is superimposed. (d) Whole-mantle cross-section, along dashed line in (c), showing mantle temperature with the velocity field (black arrows) superimposed. (e) The lateral temperature variations at 2690 km depth at $t = 848$ Ma, with the corresponding horizontal velocity field (black arrows) superimposed.

cell below the African continent (Pavoni 1992). A more recent study of the effect of lithospheric channelling suggests, however, that a single plume could explain the history of African rift volcanism (Ebinger & Sleep 1998). Studies of rifting mechanisms suggest that individual hotspot-like plumes do not play a significant direct role in the creation of intracontinental rifts, their primary role instead being the thinning and rheological weakening of the lithosphere (Ziegler 1992). An analogous view suggests that mid-ocean ridges are also the result of passive rifting driven by distant subduction-driven mantle flow (Glatzmaier *et al.* 1990) and that hotspot clusters near mid-ocean ridge axes only serve to weaken the lithosphere. These views are in accord with the model results obtained here, where the African rifting is driven by viscous coupling of the Nubia and Somalia plates to large-scale convective flow in the deep mantle.

6.3 Discussion

It is useful at this point to recapitulate the philosophy underlying the convection simulations which have been presented in this study. Our approach is based on three successive modelling steps whose coherence and consistency can be seen (Fig. 13) in the evolution of the global surface heat flux. The sequence of modelling steps are outlined as follows.

Step 1: In the reference convection model, steady state conditions with free plate motions are obtained following an initial sinusoidal temperature perturbation, which is used to start the convective processes. We do not expect to find the present-day velocity field by only imposing the geometry of the NUVEL-1 plates. Our main objective in this step is to reproduce (within 10 per cent) the present-day global constraints, namely surface heat flow,

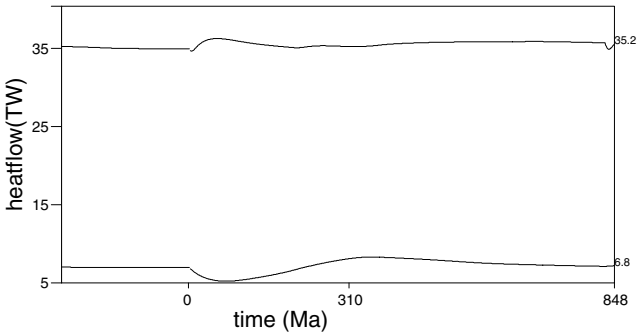

Figure 13. Time evolution of heat flow at the surface and at the CMB for the 3-step sequence of convection simulations which, respectively, include: free plate motions at steady state for $t < 0$, imposed NNR-NUVEL-1 plate motions for $t = 0$ to 829 Ma, free plate motions for $t = 829$–848 Ma.

mean plate velocity and the mean potential temperature under the plates.

Step 2: Here the reference convection model is iterated forward following the imposition of the NNR-NUVEL-1 plate motions. The iterations are continued until steady state is achieved and we find that the predicted mean global observables, especially the mean surface heat flux, are very close to those in the reference convection model.

Step 3: When the condition of prescribed plate motions is removed, the predicted plate velocities will change instantaneously in response to the internal buoyancy forces in the mantle. The global plate velocity field is, however, relatively unchanged, compared to that in step 2. Indeed, we found that by running the model forward an additional 20 Ma, we obtained almost the same plate velocity field and mantle structures (Fig. 12). The global heat flux decreases only slightly from 35.3 to 35.2 TW and this indicates that the mantle thermal structure at steady state is compatible with the surface-plate motions, whether they are imposed (as in Step 2) or free (Fig. 13).

The very small variation in mean surface heat flow (Fig. 13) throughout the sequence of three modelling steps demonstrates, on the one hand, that the initial reference model was appropriate and, on the other hand, that there is a clear consistency between the three steps, despite the changes in the surface plate boundary conditions. The main point of this approach is that the reference convection model must not only predict realistic global mean observables, as in Monnereau & Quéré (2001), but it must also yield a consistent transition to the successive modelling stages involving prescribed NUVEL-1 plate motions, followed by the removal of the surface velocity constraint, in which the plates can rotate freely again. This three-step approach was not attempted previously. By taking into account the palaeomagnetic reconstructions of plate-motion histories, our second main objective was to show that the NNR-NUVEL-1 plate motions on a 3-D time-dependent convection model are sufficient for modelling realistic hotspot generation and that the African rifting is a natural consequence of the large-scale mantle flow.

7 CONCLUSION

The convection simulations presented above have made a number of simplifying assumptions about the properties of the mantle, the most notable being the neglect of lateral (temperature-dependent) variations in rheology and the neglect of compositional heterogeneity, which could act to offset the thermally generated buoyancy forces.

The inclusion of temperature-dependent viscosity will act to further enhance the development of thermal instabilities in the hot lower thermal boundary layer at the CMB (Yuen & Peltier 1980) and this should result in an increase in the number of focused upwelling plumes (Zhong *et al.* 2000). The number of 'hotspot'-like plumes we found in the present convection simulations will, therefore, likely be a lower bound for those in the Earth. The thermal plumes that we have found (Figs 2, 4 and 5) are likely to be the most dynamically important, since their intrinsic buoyancy has allowed them to rise through the mantle even in the absence of temperature-induced reductions in their viscosity.

Recent convection simulations with compositional buoyancy show that mantle plumes will focus the intrinsically heavier mantle components in the cores of the upwelling centres but the plumes will continue to rise upwards (Zhong & Hager 2003). It is suggested that source regions for most deep plumes contain dense, low-viscosity material within D″ which will enhance their longevity (Jellinek & Manga 2004). The stability of these thermochemical 'mega-plumes' is dependent on the combination of a high viscosity region in the deep mantle and other depth-dependent parameters, such as thermal expansivity and thermal conductivity (Tackley 1998). Experimental (Davaille 1999) and joint seismic-geodynamic investigations (Forte & Mitrovica 2001) of thermochemical convection have also shown that hot upwelling structures in the lower mantle will actively ascend, despite the presence of compositional heterogeneity. The generation and subsequent ascent of focused hot upwellings are, therefore, a natural and expected characteristic of convecting systems, which have a sufficiently high component of bottom heating (either at the CMB, or at the top of a enriched compositional layer near the bottom of the mantle).

Although the effects arising from rheological and compositional complexity in the mantle are not negligible, we suggest that the most important control on the dynamics of terrestrial convection arises from the presence of surface tectonic plates. The model simulations presented here have shown the key role played by the plates in organizing and modulating the large-scale cold downwellings in the deep mantle and how these downwellings are of crucial importance in understanding the production and location of hot thermal plumes in the deep mantle.

A traditional assumption concerning the dynamics of terrestrial convection is that plumes and plates are separate and independent modes of convection (Peltier 1981; Davies & Richards 1992). This view, which holds that the mantle plume model of hotspots represents a second mode of convection, persists to this day (Foulger & Anderson 2005). Indeed, it is possible to construct spherical-shell convection models with no plates that yield hotspot plumes and models with kinematic plates and 100 per cent internal heating that do not generate any hotspot plumes. The plate-coupled convection models presented in this study provide a simple, unified framework for understanding the dynamics of cold downwellings and hot upwellings in which the latter are not a separate or independent aspect of the convecting system, but rather are complementary.

From the standpoint of the model simulations presented above, the specific results worth highlighting are:

(1) The prescription of NNR-NUVEL-1 plate motions as a surface boundary condition in a 3-D spherical model of convection leads to a mantle heat flow which is essentially identical to that obtained in a model with freely moving surface plates. Both models provide very close fits to present-day global constraints on mantle heat flow, plate-velocity speed and mantle temperature. Either model yields a reference (subadiabatic) mantle geotherm, which can be used in future studies involving tomography-based convection simulations.

(2) The number of 'hotspot'-like upwelling plumes in a model with freely moving plates (4) or in a model with prescribed NNR-NUVEL-1 plate motions (6) are close to the number (7) which has been identified for the major or primary terrestrial hotspots (Courtillot *et al.* 2003). The convection model with the NNR-NUVEL-1 plate motions predicted the 3 plumes which we associated with so-called 'isolated' hotspots (Sleep 1990), namely Hawaii, Iceland and perhaps Réunion, and in addition the predicted plumes, which we associated with the Balleny, Easter/Pitcairn and Louisville hotspots.

(3) The steady-state convection model with present-day NNR-NUVEL-1 plate motions yields a pattern of lower-mantle hotlines which closely resemble the pattern generated by a convection model run with reconstructed plate motions at $t = -119$ Ma. When the latter convection model is iterated through the entire evolution of Cenozoic plate motions, we find that the hotlines remain remarkably stable and the hotspot plumes emanating from these deep-mantle structures also remain relatively stationary. It is the apparently stable pattern of large-scale circum-Pacific subduction over the past 120 Ma that is the key to understanding the generation of similar deep-mantle hotlines and hotspots plumes in these different simulations. A practical implication of these experiments is the sufficiency of the NNR-NUVEL-1 plate motions as a surface boundary condition for generating a realistic ensemble of primary hotspots. These simulations clearly illustrate the primordial importance of the tectonic plates in controlling the evolution and pattern of temperature anomalies in the convecting mantle.

(4) The evolution of the NNR-NUVEL-1 convection model, when free surface plate motions were permitted, predicted the opening of the African plate along the Nubia–Somalia rift boundary. This rifting appeared as a natural consequence of plate coupling to deep-seated, large-scale mantle flow without requiring a sublithospheric plume directly below the rift boundary.

ACKNOWLEDGMENTS

We thank Allen McNamara and Bernhard Steinberger for very detailed and constructive reviews, which have helped to substantially clarify the arguments and results presented in this paper. We also acknowledge the contribution of Carolina Lithgow-Bertelloni who provided us with the Mesozoic–Cenozoic plate reconstructions. Support for SQ was provided by the Ontario Premier's Research Excellence Award and by the Earth-System Evolution Program of the Canadian Institute of Advanced Research. The computational infrastructure employed in the modelling presented here was funded by the Canada Foundation for Innovation. AMF also acknowledges funding provided by the Canada Research Chair program and by the Natural Sciences and Engineering Research Council of Canada.

This is GEOTOP-UQAM-McGill contribution number 2006-02.

REFERENCES

Abbott, D., Burgess, L., Longhi, J. & Smith, W.H.F., 1994. An empirical thermal history of the Earth's upper mantle, *J. geophys. Res.,* **99,** 13 835–13 850.

Anderson, D.L., 2000. The thermal state of the upper mantle: no role for mantle plumes, *Geophys. Res. Lett.,* **27,** 3623–3626.

Anderson, D., 2005. Scoring hotspots: the plume and plate paradigms, in *Plates, Plumes, Paradigms*, eds Foulger, G.R., Anderson, D.L., Natland, J.H. & Presnall D. C., Geological Society of America. Paper.

Anderson, D. & Natland, J.H., 2005. A brief history of the plume hypothesis and its competitors: concept and controversy, in *Plates, Plumes, Paradigms*, eds Foulger, G.R., Anderson, D.L., Natland, J.H. & Presnall, D.C., Geological Society of America. Paper.

Argus, D. & Gordon, R., 1991. No net rotation model of current plate velocities incorporating plate motion model NUVEL-1, *Geophys. Res. Lett.,* **18,** 2039–2042.

Boehler, R., 1992. Melting of the Fe-FeO and the Fe-FeS systems at high pressures; constraints on core temperatures, *Earth planet. Sci. Lett.,* **111,** 217–227.

Boehler, R., 1996. Melting temperature of the Earth's mantle and core: Earth's thermal structure, *Annu. Rev. Earth Planet. Sci.,* **24,** 15–40.

Bunge, H.P., Richards, M.A., Lithgow-Bertelloni, C., Baumgardner, J.R., Grand, S.P. & Romanowicz, B.A., 1998. Time scales and heterogeneous structure in geodynamic Earth models, *Science*, **280,** 91–95.

Bunge, H.P., Richards, M.A. & Baumgardner, J.R., 2002. Mantle-ciculation models with sequential data assimilation: infering present-day mantle structures from plate-motion histories, *Phil. Trans. R. Soc. Lond.,* A, **360,** 2545–2567.

Cadek, O. & Ricard, Y., 1992. Toroidal/poloidal energy partitioning and global lithospheric rotation during Cenozoic time, *Earth planet. Sci. Lett.,* **109,** 621–632.

Chapple, W.M. & Tullis, T.E., 1977. Evaluation of the forces that drive the plates, *J. geophys. Res.,* **82,** 1967–1984.

Chopelas, A. & Boehler, R., 1992. Thermal expansivity in the lower mantle, *Geophys. Res. Lett.,* **19,** 1983–1986.

Coltice, N. & Ricard, Y., 1999. Geochemical observations and one layer mantle convection, *Earth planet. Sci. Lett.,* **174,** 125–137.

Courtillot, V., Davaille, A., Besse, J. & Stock, J., 2003. Three distinct types of hotspots in the Earth's mantle, *Earth planet. Sci. Lett.,* **205,** 295–308.

Davaille, A., 1999. Simultaneous generation of hotspots and superswells by convection in a heterogeneous planetary mantle, *Nature*, **402,** 756–760.

Davaille, A., Girard, F. & Le Bars, M., 2002. How to anchor hotspots in a convecting mantle?, *Earth planet. Sci. Lett.,* **203,** 621–634.

Davies, G.F. & Richards, M.A., 1992. Mantle convection, *Journal of Geology*, **100,** 151–206.

De Mets, C.R., Gordon, R.G., Argus, D.F. & Stein, S., 1990. Current plate motions, *Geophys. J. Int.,* **101,** 425–478.

Ebinger, C.J. & Sleep, N.H., 1998. Cenozoic magmatism throughout east Africa resulting from impact of a single plume, *Nature*, **395,** 788–791.

Forsyth, D. & Uyeda, S., 1975. On the relative Importance of the Driving Forces of plate Motion, *Geophys. J. R. astr. Soc.,* **43,** 163–200.

Forte, A.M. & Peltier, W.R., 1987. Plate tectonics and aspherical Earth structure: the importance of poloidal-toroidal coupling, *J. geophys. Res.,* **92,** 3645–3679.

Forte, A.M. & Peltier, W.R., 1994. The kinematics and dynamics of poloidal-toroidal coupling in mantle flow: the importance of surface plates and lateral viscosity variations, *Adv. Geophys.,* **36,** 1–119.

Forte, A.M. & Mitrovica, J.X., 2001. Deep-mantle high-viscosity flow and thermochemical structure inferred from seismic and geodynamic data, *Nature*, **410,** 1049–1056.

Foulger, G.R. et al., 2001. Seismic tomography shows that upwelling beneath Iceland is confined to the upper mantle, *Geophys. J. Int.,* **146,** 504–530.

Foulger, G.R. & Anderson, D.L., 2005. A cool model for the Iceland hotspot, *J. Volcan. geotherm. Res.,* **141,** 122.

Furman, T., Bryce, J.G., Karson, J. & Iotti, A., 2004. East African Rift System (EARS) plume structure: insights from Quaternary Mafic Lavas of Turkana, Kenya, *J. Petrol.,* **45,** 1069–1088.

Gable, C.W., O'Connell, R.J. & Travis, B.J., 1991. Convection in three dimensions with surface plates: generation of toroidal flow, *J. geophys. Res.,* **96,** 8391–8405.

Garnero, E.J., 2000. Heterogeneity of the lowermost mantle, *Ann. Rev. Earth Planet. Sci.,* **28,** 509–537.

Glatzmaier, G.A., Schubert, G. & Bercovici, D., 1990. Chaotic, subduction-like down flows in a spherical model of convection in the Earth's mantle, *Nature*, **347,** 274–277.

Glatzmaier, G.A., Coe, R.S., Hongre, L. & Roberts, P.H., 1999. The role of the Earth's mantle in controlling the frequency of geomagnetic reversals, *Nature*, **401,** 885–890.

Gonnermann, H.M., Jellinek, A.M., Richards, M.A. & Manga, M., 2004. Modulation of mantle plumes and heat flow at the core mantle boundary by plate-scale flow: results from laboratory experiments, *Earth planet. Sci. Lett.,* **226,** 53–67.

Grand, S.P., 2002. Mantle shear-wave tomography and the fate of subducted slabs, *Phil. Trans. R. Soc. Lond.,* A, **360,** 2475–2491.

Gripp, A.E. & Gordon, R.G., 2002. Young tracks of hotspots and current plate velocities, *Geophys. J. Int.,* **150,** 321–361.

Gurnis, M., Mitrovica, J.X., Ritsema, J. & van Heijst, H.J., 2000. Constraining mantle density structure using geological evidence of surface uplift rates: the case of the African superplume, *Geochem. Geophys. Geosystems*, **1,** 1999GC000035.

Hager, B.H. & O'Connell, R.J., 1981. A simple global model of plate dynamics and mantle convection, *J. geophys. Res.,* **86,** 4843–4867.

Hager, B.H., 1984. Subducted slabs and the geoid: constraints on mantle rheology and flow, *J. geophys. Res.,* **89,** 6003–6016.

Harper, J.F., 1986. Mantle flow and plate motions, *Geophys. J. R. astr. Soc.,* **87,** 155–171.

Helmberger, D.V., Wen, L. & Ping, X., 1998. Seismic evidence that the source of the Iceland hotspot lies at the cmb, *Nature*, **396,** 252–255.

Jarvis, G.T., 1993. Effects of curvature on two-dimensional models of mantle convection: cylindrical polar coordinates, *J. geophys. Res.,* **98,** 4477–4486.

Jeffreys, H., 1930. The instability of a compressible fluid heated below, *Proc. Camb. Phil Soc.,* **26,** 170–172.

Jellinek, A.M. & Manga, M., 2002. The influence of a chemical boundary layer on the fixity, spacing and lifetime of mantle plumes, *Nature*, **418,** 760–763.

Jellinek, A.M. & Manga, M., 2004. Links between long-lived hot spots, mantle plumes, D″, and plate tectonics, *Rev. Geophys.,* **42,** No.3, RG3002, doi:10.1029/2003RG00144, 14 September 2004.

Keller, W.R., Anderson, D.L. & Clayton, R.W., 2000. Resolution of tomographic models of the mantle beneath Iceland, *Geophys. Res. Lett.,* **27,** 3993–3996.

Kreemer, C., Holt, W.E. & Haines, A.J., 2003. An integrated global model of present-day plate motions and plate boundary deformation, *Geophys. J. Int.,* **154,** 8–34.

Labrosse, S., 2002. Hotspots, mantle plumes and core heat loss, *Earth Planet. Sci. Lett.,* **199,** 147–156.

Li, X., Kind, R., Priestly, K., Sobolev, S.V., Tilman, F., Yuan, X. & Weber, M., 2000. Mapping the Hawaiian plume conduit with converted seismic waves, *Nature*, **405,** 938–941.

Lithgow-Bertelloni, C. & Richards, M., 1998. The dynamics of Cenozoic and Mesozoic plate motions, *Rev. Geophys.,* **36,** 27–78.

Lowman, J.P., King, S.D. & Gable, C.W., 2001. The influence of tectonic plates on mantle convection patterns, temperature and heat flow, *Geophys. J. Int.,* **146,** 619–636.

Mitrovica, J.X. & Forte, A.M., 2004. A new inference of mantle viscosity based upon joint inversion of convection and glacial isostatic adjustment data, *Earth planet. Sci. Lett.,* **225,** 177–189.

Molnar, P. & Stock, J, 1987. Relative motion of hotspots in the Pacific Atlantic and Indian Oceans since Late Cretaceous time, *Nature*, **327,** 587–591.

Monnereau, M. & Quéré, S., 2001. Spherical shell models of mantle convection with tectonic plates, *Earth planet. Sci. Lett.,* **184,** 575–587.

Montelli, R., Nolet, G., Dahlen, F.A., Masters, G., Engdahl, E.R. & Hung, S.-H., 2004. Finite-frequency tomography reveals a variety of plumes in the mantle, *Science*, **303,** 338–343.

Morgan, W.J., 1971. Convection plumes in the lower mantle, *Nature*, **230,** 42–43.

Morgan, W.J., 1972. Deep mantle convection plumes and plate motions, *Bull. Am. Assoc. Pet. Geol.,* **56,** 203–213.

Nataf, H.-C., 2000. Seismic imaging of mantle plumes, *Ann. Rev. Earth Planet. Sci.,* **28,** 391–417.

Nimmo, F., Price, G.D., Brodholt, J. & Gubbins, D., 2004. The influence of potassium on core and geodynamo evolution, *Geophys. J. Int.,* **156,** 363–376.

Norton, I.O., 1995. Plate motions in the North Pacific: the 43 Ma non event, *Tectonics*, **14,** 1080–1094.

Parsons, B. & Sclater, J.G., 1977. An analysis of the variation of ocean floor bathymetry and heat flow with age, *J. Geophys. Res.,* **82,** 803–826.

Pavoni, N., 1992. Rifting of Africa and pattern of mantle convection beneath the African plate, *Tectonophysics*, **215,** 35–53.

Peltier, W.R., 1981. Surface plates and thermal plumes: separate scales of the mantle convective circulation, in '*The Evolution of the Earth*', pp. 229–248, eds O'Connell, R.J. & Fyfe, W., AGU (Washington, DC).

Pollack, H.N., Hurter, S.J. & Johnston, J.R., 1993. Heat loss from the earth's interior: analysis of the global data set, *Rev. Geophys.,* **31,** 267–280.

Ricard, Y. & Vigny, C., 1989. Mantle dynamics with induced plate tectonics, *J. geophys. Res.,* **94,** 17 543–17 559.

Ricard, Y., Doglioni, C. & Sabadini, R., 1991. Differential rotation between lithosphere and mantle: a consequence of lateral mantle viscosity variations, *J. geophys. Res.,* **96,** 8407–8415.

Richards, M.A., Hager, B.H. & Sleep, N.H., 1988. Dynamically supported geoid highs over hotspots: observation and theory, *J. geophys. Res.,* **93,** 7690–7708.

Russell, S.A., Lay, T. & Garnero, E.J., 1998. Seismic evidence for small-scale dynamics in the lowermost mantle at the root of the Hawaïan hotspot, *Nature*, **396,** 255.

Schaeffer, N. & Manga, M., 2001. Interaction of rising and sinking mantle plumes, *Geophys. Res. Lett.,* **28,** 455–458.

Sclater, J.G., Jaupart, C. & Galson, D., 1980. The heat flow through oceanic and continental crust and the heat loss of the Earth, *Rev. Geophys. Space Phys.,* **18,** 269–311.

Shen, Y., Solomon, S.C., Bjarnason, I.T. & Wolfe, C.J., 1998. Seismic evidence for a lower-mantle origin of the Iceland plume, *Nature*, **395,** 62–65.

Sleep, N.H., 1990. Hotspots and mantle plumes: some phenomenology, *J. geophys. Res.,* **95,** 6715–6736.

Stacey, F.D, 1992. *Physics of the Earth*, 3rd edn, p. 301, Brookfield, Brisbane.

Stacey, F.D. & Loper, D.E., 1988. Thermal history of the Earth: a corollary concerning non-linear mantle rheology, *Phys. Earth. planet. Inter.,* **53,** 167–174.

Stein, C.A., 1995. Heat Flow of the Earth, in *'Global Earth Physics: A Handbook of Physical Constants'* (AGU Reference Shelf 1), 144–158.

Stein, C.A. & Stein, S., 1992. A model for the global variation in oceanic depth and heat flow with lithospheric age, *Nature*, **359,** 123–129.

Steinberger, B. & O'Connell, R.J., 1998. Advection of plumes in mantle flow: implications for hotspot motion, mantle viscosity and plume distribution, *Geophys. J. Int.,* **132,** 412–434.

Storey, B.C., 1995. The role of mantle plumes in continental breakup: case histories from Gondwanaland, *Nature*, **377,** 301.

Tackley, R.J., 1998. Three-dimensional simulations of mantle convection with a thermochemical basal boundary layer: D″?, in *The Core-Mantle-Boundary region*, pp. 231–253, eds Gurnis *et al.*, AGU, Washington, DC.

Tarduno, J.A. & Gee, J., 1995. Large-scale motion between Pacific and Atlantic hotspots, *Nature*, **378,** 477–480.

van der Voo, R., Spakmann, W. & Bijwaard, H., 1999. Tethyan subducted slabs under India, *Earth planet. Sci. Lett.,* **171,** 7–20.

Whitehead, J.A., 1988. Fluid models of geological hotspots, *Ann. Rev. Fluid Mech.,* **20,** 61–87.

Wilson, J.T., 1963. A possible origin of the Hawaiian Islands, *Can. J. Phys.,* **41,** 863–870.

Wolfe, C.J., Bjarnason, I.T., VanDecar, J.C. & Solomon, S.C., 1997. Seismic structure of the Iceland mantle plume, *Nature*, **385,** 245–247.

Yuen, D.A. & Peltier, W.R.., 1980. Mantle plumes and the thermal stability of the D″ layer, *Geophys. Res. Lett.,* **7,** 625–628.

Zhong, S. & Hager, B.H., 2003. Entrainment of a dense layer by thermal plumes, *Geophys. J. Int.,* **154,** 666–676.

Zhong, S., Zuber, M.T., Moresi, L. & Gurnis, M., 2000. Role of temperature-dependent viscosity and surface plates in spherical shell models of mantle convection, *J. geophys. Res.,* **105,** 11 063–11 082.

Ziegler, P.A., 1992. Plate tectonics, plate moving mechanisms and rifting, *Tectonophys.,* **215,** 9–34.

Zoback, M.L. et al., 1989. Global patterns of tectonic stress, *Nature*, **341,** 291–298.